SHADOW DETECTION AND COMPENSATION IN AERIAL IMAGES WITH AN APPLICATION TO BUILDING HEIGHT ESTIMATION

A THESIS SUBMITTED TO
THE GRADUATE SCHOOL OF NATURAL AND APPLIED SCIENCES
OF
MIDDLE EAST TECHNICAL UNIVERSITY

BY

AHMET ŞEREF

IN PARTIAL FULFILLMENT OF THE REQUIREMENTS
FOR
THE DEGREE OF MASTER OF SCIENCE
IN
ELECTRICAL AND ELECTRONICS ENGINEERING

SEPTEMBER 2010

Approval of the thesis:

SHADOW DETECTION AND COMPENSATION IN AERIAL IMAGES WITH AN APPLICATION TO BUILDING HEIGHT ESTIMATION

submitted by **AHMET ŞEREF** in partial fulfillment of the requirements for the degree of **Master of Science in Electrical and Electronics Engineering Department, Middle East Technical University** by,

Prof. Dr. Canan Özgen _____
Dean, Graduate School of **Natural and Applied Sciences**

Prof. Dr. İsmet Erkmen _____
Head of Department, **Electrical and Electronics Engineering**

Assoc. Prof. Dr. A. Aydın Alatan _____
Supervisor, **Electrical and Electronics Engineering Dept., METU**

Examining Committee Members:

Prof. Dr. Gözde Bozdağı Akar _____
Electrical and Electronics Engineering Dept., METU

Assoc. Prof. Dr. A. Aydın Alatan _____
Electrical and Electronics Engineering Dept., METU

Assoc. Prof. Dr. Şebnem Düzgün _____
Geodetic and Geographic Information Tech. Dept., METU

Assist. Prof. Dr. Afşar Saranlı _____
Electrical and Electronics Engineering Dept., METU

Assist. Prof. Dr. İlkay Ulusoy _____
Electrical and Electronics Engineering Dept., METU

Date: _____

I hereby declare that all information in this document has been obtained and presented in accordance with academic rules and ethical conduct. I also declare that, as required by these rules and conduct, I have fully cited and referenced all material and results that are not original to this work.

Name, Last Name : Ahmet ŞEREF

Signature :

ABSTRACT

SHADOW DETECTION AND COMPENSATION IN AERIAL IMAGES WITH AN APPLICATION TO BUILDING HEIGHT ESTIMATION

Şeref, Ahmet
M.S., Department of Electrical and Electronics Engineering
Supervisor: Assoc. Prof. Dr. A. Aydın Alatan

September 2010, 104 pages

This thesis is devoted to the shadow detection and compensation in aerial images with application of the detection results to building height detection. Shadows could be defined as the parts of the scene that is not directly illuminated by a light source due to obstructing object or objects. Usually the shadows in images or video are undesirable, since they could cause degradation of the expected results during processing of the image or video for object detection, segmentation, scene surveillance or similar purposes. However shadow information could also be used for beneficial purposes like revealing information about the object's shape, orientation and even about the light source. In this thesis firstly shadow detection methods are overviewed. Beside the selected methods from literature, some novel approaches are also proposed and experimented. Then shadow compensation methods are overviewed and experimented. Finally an example of beneficial utilizations of shadow information is studied, where buildings' heights are estimated from their shadow length and sun angles.

Keywords: Shadow detection, aerial and satellite images, shadow compensation, building height estimation.

ÖZ

HAVA FOTOĞRAFLARINDA GÖLGE TESPİTİ VE DÜZELTİLMESİNİN BİNA YÜKSEKLİĞİ HESAPLAMASINA UYGULAMASI

Şeref, Ahmet
Yüksek Lisans, Elektrik ve Elektronik Mühendisliği Bölümü
Tez Yöneticisi: Doç. Dr. A. Aydın Alatan

Eylül 2010, 104 sayfa

Bu tez, hava fotoğraflarında gölge tespiti, düzeltme ve bunun uygulaması olarak bina yüksekliği tahmini üzerine bir çalışmadır. Gölge bir sahnede bazı nesne veya nesnelerin engel olması ile doğrudan ışık kaynağı tarafından aydınlatılmayan kısımlar olarak tanımlanabilir. Gölgeler, nesne bulma, bölümleme, olay yeri gözetleme ve benzeri resim ve video kaynaklı işlemlerde beklenen sonuçlar üzerinde olumsuz etki yaratacağından, resimlerde ve videolarda genellikle istenmeyen durumlardır. Bununla birlikte gölgeler, nesne şekli, durumu ve hatta ışık kaynağı ile ilgili bilgiler gibi faydalı bilgilere ulaşmak amaçlı kullanılabilir. Bu tez çalışmasında ilk olarak gölge algılama yöntemleri incelenmiştir. Literatürdeki bazı yöntemler yanı sıra ve yeni önerilen bazı yaklaşımlar tecrübe edilmiştir. Sonrasında literatürdeki gölge düzeltme yöntemleri incelenmiş ve örnek resimler üzerinde deneyler yapılmıştır. Son olarak, tespit edilen gölge bilgisinin faydalı bir kullanımına örnek olarak, güneş ve uydu yükseliş ve istikamet açılarını kullanmak sureti ile gölge uzunluğundan bina yüksekliği tahmini çalışması yapılmıştır.

Anahtar kelimeler: Gölge algılama, hava ve uydu fotoğrafları, gölge düzeltme, bina yükseklik tahmini

ACKNOWLEDGEMENTS

I would like to express my appreciation to my supervisor Assoc. Prof. Dr. A. Aydın Alatan, for his guidance and positive suggestions throughout this thesis study. Besides his technical assistance, cheerful and sincere personality of him also motivated me a lot during this study.

I would like to also thank to my friend Onur Ali Demirkol, for his friendship, motivation and assistance during the courses that we attend together.

I would like to also express my love and thanks to my dear wife Ebru, for her patience and support during the master study.

Finally, I would like to thank my parents for their endless love and support over the years.

TABLE OF CONTENTS

LIST OF TABLES

TABLES

LIST OF FIGURES

FIGURES

CHAPTER 1

INTRODUCTION

The shadow detection and compensation is an important issue in machine vision systems for many purposes. Shadows in an image may reveal information about the objects shape, orientation and even about the light source. A typical utilization might be given as detecting a building's height from its shadow [44], [45], [46], [56], [57]. Another example to beneficial usage of shadow information is the thesis study of Güler [21] on post event photographs of earthquake damaged scenes. There are also other studies [20], [24].

However, usually the shadows in images or video are undesirable, since they could cause degradation of the output during processing of the image or video for object detection, segmentation, scene surveillance or similar purposes. Shadows in an image can modify a target object's shape to be detected. To prevent this problem shadows should be detected in order to separate those from target object [8].

There are mainly two domains that are covered in this study where shadow detection and compensation algorithms applied. One domain consists of image sequences, namely video content, whereas the second one is about static images.

For the first case, the main purpose is usually change detection, scene matching or surveillance. Background subtraction is a common technique for obtaining the target object. However, without shadow detection, background subtraction might not be sufficient, since shadows usually affects the performance in a negative way for these purposes. For example, a shadow of an object in a traffic surveillance camera might be detected as

the part of the object or even two objects may be detected as one object, if they are nearby and moving at the same direction and the shadow of one of them is falling over the other.

For the second case, i.e. static images, main purpose might be detection of a specific target. The shadows residing in the processed image will result in changed geometric shapes of the objects; thus, maybe avoiding the detection of a target.

The researches and studies about shadow detection and compensation is mainly done in the last decade. However, there are also important studies in 90s, such as [13], [38].

1.1 Scope of the Thesis

This thesis mainly deals with shadow detection. Beside shadow detection the thesis branches into two subjects, where the shadow detection output is utilized. The first one is shadow compensation. The second one is building height estimation from its shadow.

Shadow detection on aerial images are concentrated on this thesis study, so shadow detection on dynamic scenes which is referred as moving shadow detection [5] is beyond the scope of this thesis. Some of the static scene shadow detection methods are tested on sample images and the results are compared. Cloud and cloud shadow detection is also another study field in aerial images. Some example studies are [40], [41] and [49]. The cloud and cloud shadow detection and its compensation is out of scope of this study.

Shadow compensation methods are overviewed and histogram matching, gamma correction and linear correlation based compensation methods are tested on the sample images, which are outputs of the shadow detection algorithms that are experimented.

Building height estimation is selected as an example application field, where shadow detection output is used. In building height estimation, shadow length is first determined and then by using the sun and satellite angles

building height is estimated. Building corners are assumed to be available for the process; the building detection is beyond the scope of this thesis.

1.2 Outline of the Thesis

In Chapter 2, shadow and color definitions are given. Then color spaces that are mentioned in this thesis are explained.

In Chapter 3, shadow features are firstly explained and observed on some sample images. Secondly shadow detection methods are overviewed followed by detail explanation of compared shadow detection methods. Then experimental results are given and the experimental results are discussed.

In Chapter 4, shadow compensation methods are overviewed and some methods are compared. The experimental results are discussed at the end of the chapter.

In Chapter 5, an example application of shadow detection is mentioned: Building height estimation from shadow length. Building height estimation is done by using detected shadow length with sun and satellite angle information of the image processed. Some sample scenes are used for the experiment. The results are discussed at the end of the chapter.

The thesis is concluded with Chapter 6, with discussion of all the observed results of shadow detection, compensation and its application to building height detection.

CHAPTER 2

DEFINITIONS AND COLOR SPACES

In this chapter, shadow and shadow types are introduced as a first step. Secondly, color definition is given and followed by color models descriptions, since the shadow detection and restoration requires complete understanding of the color spaces.

2.1 Definition of the Shadow

Shadows could be defined as the parts of the scene that is not directly illuminated by a light source due to an obstructing object or objects. The shadow regions, however, are illuminated by ambient light. Similar definition for the shadow is given in some of the shadow detection literature [3], [8], [13], [15], [38].

A typical shadow could be divided into 2 different types. One type is denoted as *self shadow* where the shadow region is on the object itself. The other type is *cast shadow* for which the shadow region is on the background or on another objects. The cast shadow is usually further divided into 2 parts, *umbra* and *penumbra* [3], [28], [38].

In [28], Dare defined the umbra and penumbra regions as follows: “The umbra represents the shadow region where the primary light source is completely obscured; whereas the penumbra is the region around the edge of a shadow where the light source is only partially obscured.”

Jiang and Ward [38] mentioned that a point light source will generate only umbra while an area light source will generated also penumbra and they

argued that a thin penumbra may not be appear in the image due to digitizing effects.

In Figure 1, the shadow types are shown and in Figure 2, umbra and penumbra are depicted.

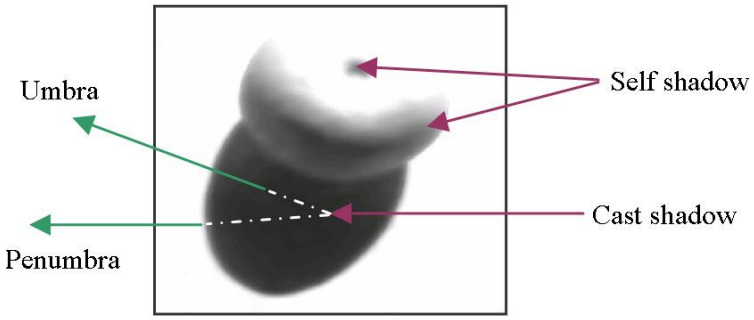

Figure 1 – Shadow types [3]

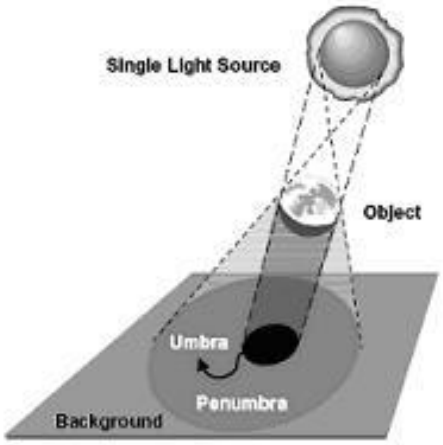

Figure 2 – Umbra and Penumbra illustration [26]

2.2 Definition of the Color

Every object in the nature absorbs some part of light from an illumination source and reflects some wavelengths. When perceived by our eyes, this phenomenon will be sensed as the color of that object. Gonzales and Woods [54] mentioned that the perceiving and interpreting colors by human brain is still not fully understood, however, color physical nature could be based on experimental and theoretical results.

The CIE (Commission Internationale de l'EcIairage — The International Commission on Illumination) brings a standard definition of primary colors wavelengths in 1931: Blue = 435.8 nm, Green = 546.1 nm and Red = 700nm [54].

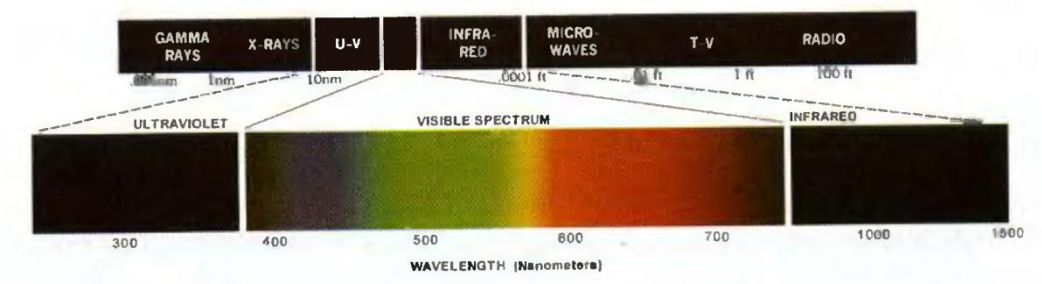

Figure 3 – Wavelengths comprising the visible range of the electromagnetic spectrum [54]

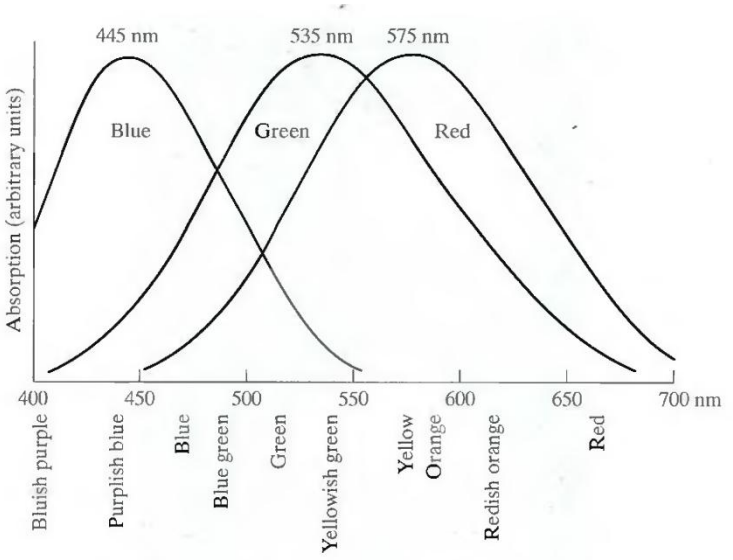

Figure 4 – Absorption of light by the red, green, and blue cones in the human eye as a function of wavelength [54]

2.3 Color Spaces

A *color space* is a specification of colors in some standard way. It is also referred as color model. Each color could be represented by a point in any of the color spaces [54]. There are different color models that each differs by their approach of specifying a color. Some important color models are defined in the following sections:

2.2.1 RGB Color Space

The RGB color model is an additive color model which means any color could be defined by addition of the primary colors. Red, Green and Blue are the primary colors of light. In this color space, each component represents Red, Green and Blue channel [54].

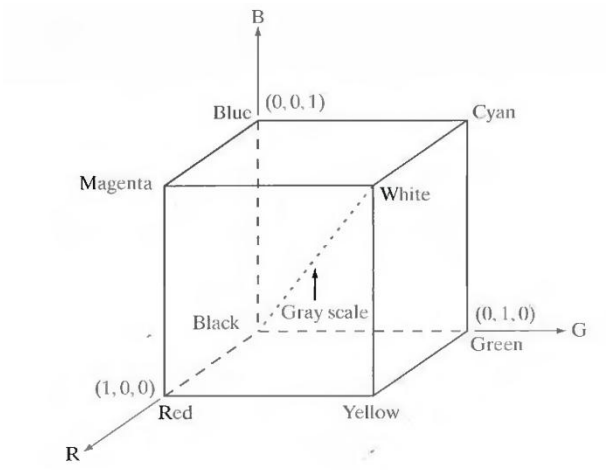

Figure 5 – RGB Color Cube [54]

RGB color space is usually accepted as non-appropriate for color image processing applications due to the following major drawbacks [17]:

- It is device dependent and excludes some visible colors
- Perceptually non-uniform and distance metric will not represent the real differences between colors
- Difficult to find thresholds for RGB cube

Hence, there are other color spaces defined by the researchers.

2.2.1 HSV/HSI Color Spaces

The Hue-Saturation-Value (HSV) and Hue-Saturation-Intensity (HSI) color spaces are similar. These color spaces are similar to human description of a color [54].

Since they can be obtained by a linear transformation from the RGB color space, they inherit drawbacks from RGB color space. For example, they are also device dependent and non-uniform.

Hue component defines the color which corresponds to the dominant color that is perceived. Saturation is defined as purity of the hue or strength of the color. These two components together define the chromaticity. On the other hand value or intensity component defines the intensity [54].

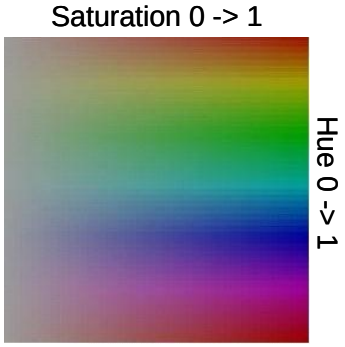

Figure 6 – Hue and Saturation Depiction

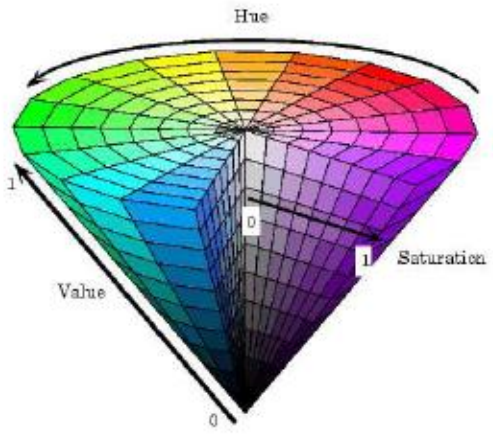

Figure 7 – Hue, Saturation and Value components (www.mathworks.com)

2.2.1.1 HSV Color Space

In HSV color space, the conversion from RGB color space is obtained as follows [54]:

$$H = \cos^{-1}\left(\frac{0.5\,x\,(R-G) + (R-B)}{\sqrt{((R-G)^2 + (R-B)x(G-B))}}\right) \qquad (2.1)$$

$$S = \frac{\max(R,G,B) - \min(R,G,B)}{\max(R,G,B)} \qquad (2.2)$$

$$V = \max(R,G,B) \qquad (2.3)$$

2.2.1.2 HSI Color Space

In HSI color space, the conversion from RGB color space is achieved as follows [54]:

$$H = \begin{cases} \theta & if\ B \le G \\ 360 - \theta & if\ B > G \end{cases} \qquad (2.4)$$

$$\theta = \cos^{-1}\left\{\frac{\frac{1}{2}[(R-G) + (R-B)]}{[(R-G)\text{^}2 + (R-B)x(G-B)]^{1/2}}\right\} \qquad (2.5)$$

$$S = 1 - \frac{3}{(R+G+B)}\,[\min(R,G,B)] \qquad (2.6)$$

$$I = \frac{1}{3}\,(R+G+B) \qquad (2.7)$$

2.2.2 YIQ Color Space

In YIQ color space, the Y represents luminance information; I and Q represent the color information. This color space is used in National Television Standards Commission (NTSC) which is a color television broadcast standard mostly used in America and Japan [34]. The conversion from RGB color space is given below [43]:

$$\begin{bmatrix} Y \\ I \\ Q \end{bmatrix} = \begin{bmatrix} 0.299 & 0.587 & 0.114 \\ 0.596 & -0.274 & -0.322 \\ 0.211 & -0.523 & 0.312 \end{bmatrix} \begin{bmatrix} R \\ G \\ B \end{bmatrix} \quad (2.8)$$

2.2.3 $C_1C_2C_3$ Color Space

The $C_1C_2C_3$ color space is introduced in [42]. This color space is referred as being invariant to shadows and shading [8], [9].

The conversion from RGB color space is as follows:

$$C_1 = \arctan\left(\frac{R}{max(G,B)}\right) \quad (2.9)$$

$$C_2 = \arctan\left(\frac{G}{max(R,B)}\right) \quad (2.10)$$

$$C_3 = \arctan\left(\frac{B}{max(G,R)}\right) \quad (2.11)$$

2.2.4 YC_bC_r Color Space

In YC_bC_r color space, the Y represents luminance information; C_b and C_r represent the color information. This color space is mostly used in video and image compression standards like JPEG and MPEG [34].

The conversion from RGB color space is given below [43]:

$$\begin{bmatrix} Y \\ C_b \\ C_r \end{bmatrix} = \begin{bmatrix} 16 \\ 128 \\ 128 \end{bmatrix} + \begin{bmatrix} 65.481 & 128.553 & 24.966 \\ -37.797 & -74.203 & 112 \\ 112 & -93.786 & -18.214 \end{bmatrix} \begin{bmatrix} R \\ G \\ B \end{bmatrix} \quad (2.12)$$

CHAPTER 3

SHADOW DETECTION

The shadow detection process could be a primary step for compensation of the shadows and followed by an eventual step of image analysis task, such as object recognition or it could be a fundamental step where the detection results are directly used by 3D shape estimation or similar tasks. In any case, shadow detection is an initial process for a final image analysis task. Hence, the performance of the final task is highly dependent on the shadow detection performance.

In this chapter, some feature-based shadow detection methods are analyzed and they are compared by the help of some experimental results.

3.1 Shadow Features

In this section, shadow features are analyzed. Changes in shadow are analyzed on image samples, which are colored as Yellow, Black, Blue, Green, Red and White. The sample images are given in Figure 8. An example setup of these sample pictures is given in Figure 9. In these setups a uniform colored paper is laid on the surface, an obstructing object is set beside to the side of the sun light and a shadowed part is obtained. Then by using a photo editor program the sample images are cropped. No further image processing or filtering is applied to preserve original color on the sample image.

Figure 8 – Sample images that are used for shadow feature analyses

Figure 9 – An example to setup for extracting sample images

3.1.1 Changes in RGB Color Space Components with Shadow

The chromatic profiles for the images in Figure 8 are plotted in Figure 10, respectively for R, G and B:

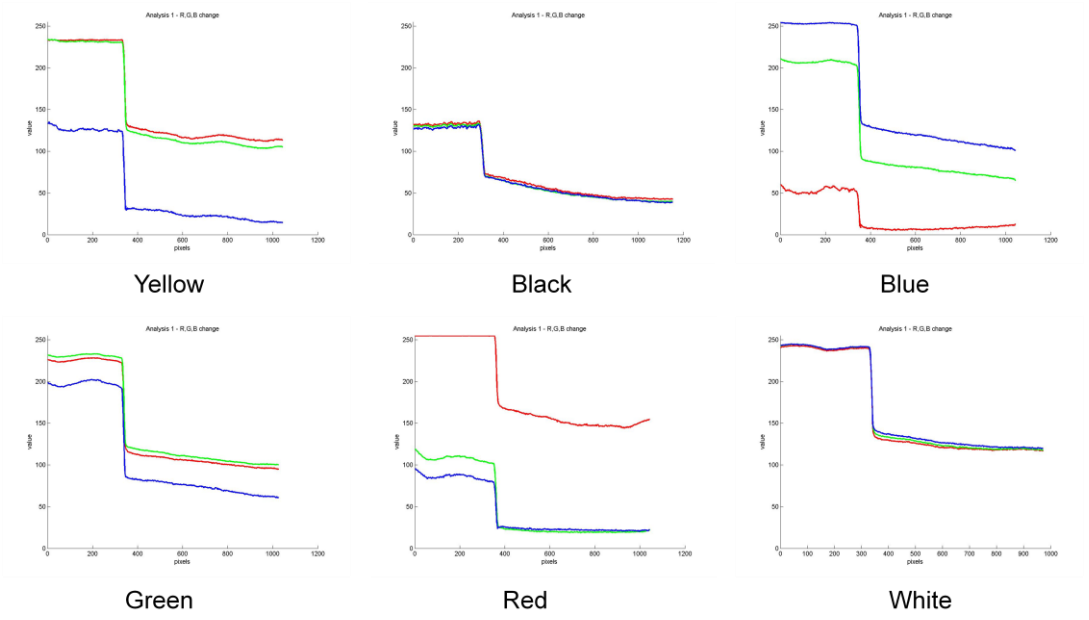

Figure 10 – R,G and B values change between shadow and non-shadow regions for sample images in Figure 8

As expected, all three (R, G, B) components are attenuated, since the illumination is smaller in the shadowed part. Another expected and observed issue is, the most dominant component or components are attenuated but being still dominant, thus still preserving the color information under shadow.

In white image sample an important issue is also observed, which indicates that red component is the most attenuated, whereas blue is the least

attenuated component. This issue is known as Rayleigh Scattering effect and is also referenced in the literature as follows:

Golden et al. mentioned that the scenes where the illumination source is mainly sky light the shadowed areas spectrum is not only dimmer but also skewed to blue-violet wavelengths [11].

Huang et al. [36] analyzed this issue as a physical phenomenon as below:

The following equation which is given by mentioning that it could be considered that change for the shadowed areas in images is only the diffusion part of the Phong's illumination model [37], since the images are matt and dull. Hence, the R, G and B value changes are given as:

$$\Delta I_R = \int K_d(\lambda).I_I(\lambda).S_R(\lambda).\cos\theta \; d\lambda \qquad (3.1)$$

$$\Delta I_G = \int K_d(\lambda).I_I(\lambda).S_G(\lambda).\cos\theta \; d\lambda \qquad (3.2)$$

$$\Delta I_B = \int K_d(\lambda).I_I(\lambda).S_B(\lambda).\cos\theta \; d\lambda \qquad (3.3)$$

where *ΔIs* are the changes in R, G and B components, *I* is the radiance, *Θ* is the incident angle of the light source, *S*(*λ*) are color filters of the camera and *K*(*λ*) are the albedo of the surface [36].

If *K*(*λ*) are considered to be the constant for all wavelengths, then;

$$\int I_I(\lambda).S_R(\lambda) \; d\lambda = \int I_I(\lambda).S_G(\lambda) \; d\lambda = \int I_I(\lambda).S_B(\lambda) \; d\lambda \quad (3.4)$$

and thus;

$$\Delta I_R = \Delta I_G = \Delta I_B \qquad (3.5)$$

meaning that all three components are attenuated with the same ratio [36].

However, it is mentioned that $K(\lambda)$ values are positive proportional to the wavelength; hence, the below equation should hold;

$$\int K_d(\lambda).I_I(\lambda).S_R(\lambda)\ d\lambda\ > \int K_d(\lambda).I_I(\lambda).S_R(\lambda)\ d\lambda > \int K_d(\lambda).I_I(\lambda).S_R(\lambda)\ d\lambda \qquad (3.6)$$

which results with following relation;

$$\Delta I_R > \Delta I_G > \Delta I_B \qquad (3.7)$$

The above relation states that the red component is the most attenuated and the blue component is the least attenuated one in shadow region [36].

3.1.2 Changes in HSV Color Space Components with Shadow

As a second analysis, H, S and V component profiles within and outside shadow regions are also analyzed. In below figure, hue is depicted with red lines, Saturation is depicted with green lines and Value is depicted with blue lines:

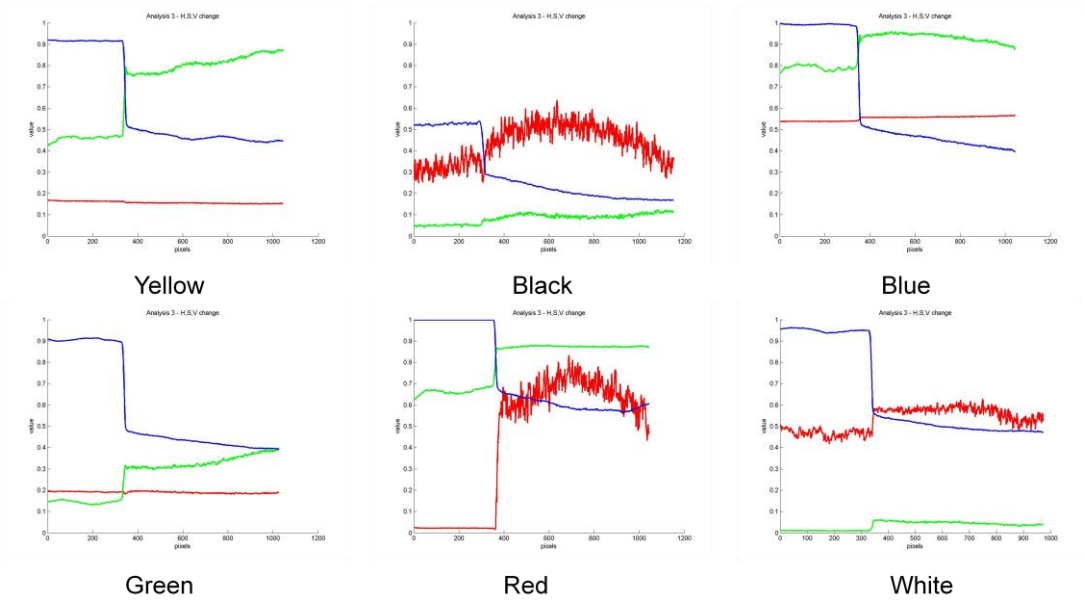

Figure 11 – H,S and V values change between shadow and non-shadow regions for sample images in Figure 8

As we analyze the results, we observe that Value component decreases for all cases as expected since the illumination decreases. In contrast Saturation values tend to increase for all cases. Hue component remains constant for yellow, green and blue colors and increases for red, white and black colors.

3.1.3 Changes in YIQ Color Space Components with Shadow

As a third analysis, Y, I and Q component profiles in YIQ color space within and outside shadow regions are also analyzed. In Figure 12, Y is depicted with red lines, I is depicted with green lines and Q is depicted with blue lines:

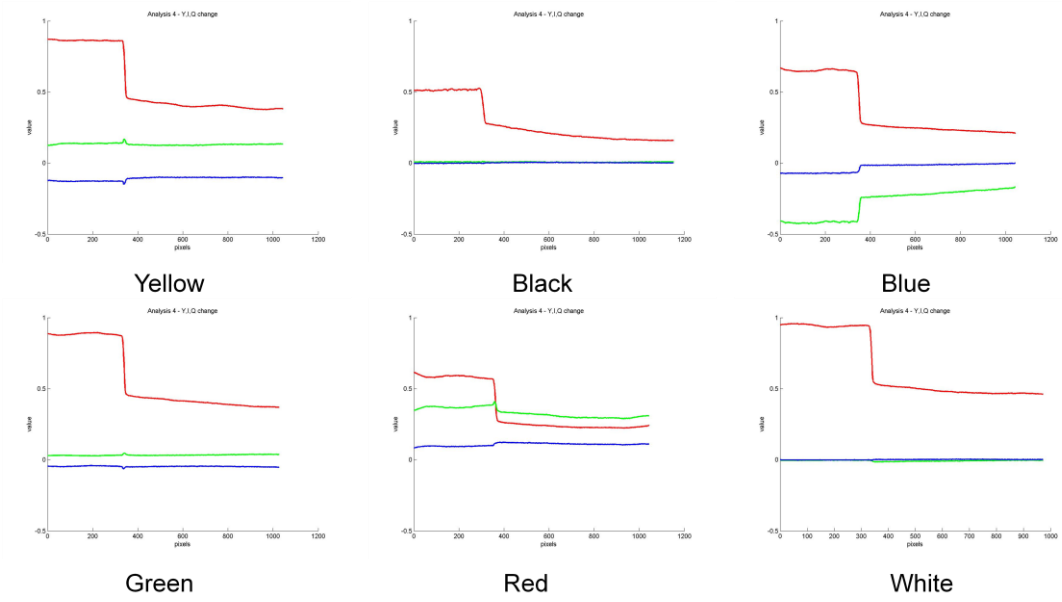

Figure 12 – Y,I and Q values change between shadow and non-shadow regions for sample images in Figure 8

As we analyze the results, we observe that Y component that represents the luminance is decreased for all cases as expected. However I and Q components that represent the color information, remains almost constant for all cases.

3.1.4 Changes in $C_1C_2C_3$ Color Space Components with Shadow

As a final analysis, $C_1C_2C_3$ component profiles within and outside shadow regions are also analyzed. In Figure 13, C_1 is depicted with red lines, C_2 is depicted with green lines and C_3 is depicted with blue lines:

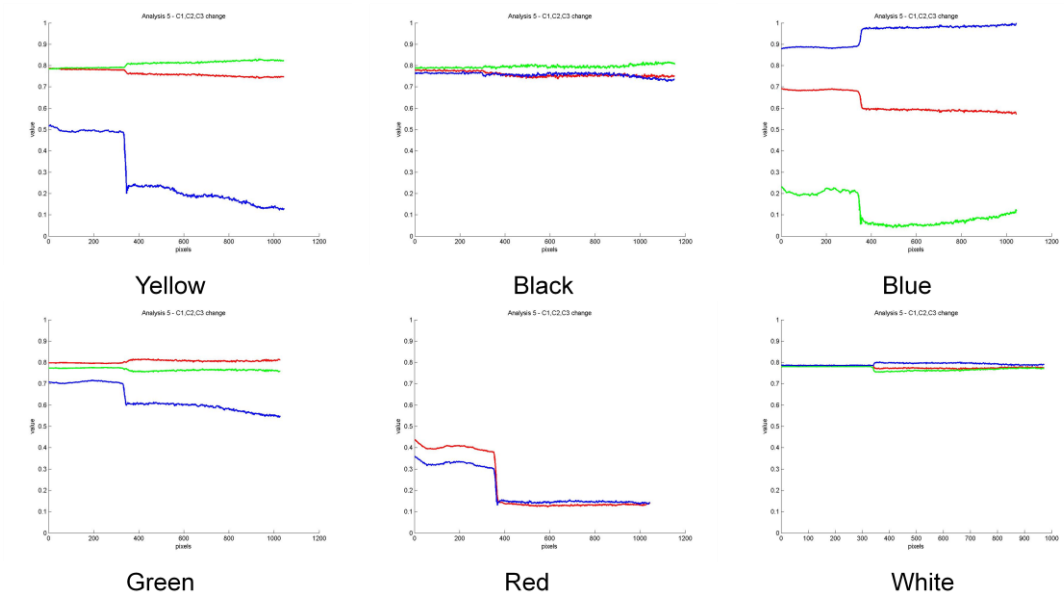

Figure 13 – C_1,C_2 and C_3 values change between shadow and non-shadow regions for sample images in Figure 8

As we analyze the results, a beneficial deduction could not have been obtained.

3.2 Overview of Shadow Detection Methods

Shadow detection methods could be classified according to the input data. The work in the literature could be divided into two classes, one class deals with moving shadow detection while the other class deals with static image shadow detection.

3.2.1 Moving Shadow Detection

Shadow detection in dynamic scenes are referred as *moving shadow detection* [5] and usually their detection approach and steps are different from non-dynamic scenes (still images).

Also the purpose for the shadow detection in dynamic scenes could be change detection, scene matching or surveillance that is different than a

detection purpose for images. In moving shadow detection methods generally a background subtraction step is usually present [5].

There are several studies on moving shadow detection. Some example works are [5], [6], [12], [18], [19], [22], [23] and [25]. Prati et al. compared moving shadow algorithms in [50].

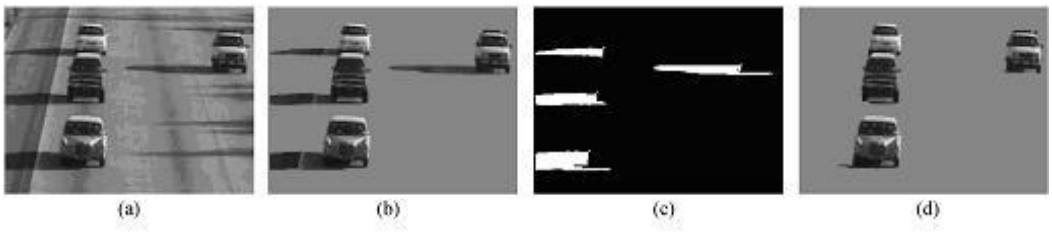

Figure 14 – Moving shadow detection and foreground detection result [5]

3.2.2 Static Shadow Detection

Shadow detection in images has usually different purposes than moving shadow detection as mentioned previously. In static shadow detection, the purpose could be estimation of objects shape from its detected shadow or an intermediate step to image enhancement for pattern or object recognition or similar purposes.

Static shadow detection methods could be further classified into *model-based* and *feature-based* [4], [8], [47].

3.2.2.1 Model-based Shadow Detection

In model-based shadow detection, apart from the input image geometrical information of the scene, for example digital surface model (DSM) as well as

light source information for example sun elevation and azimuth angles are also utilized. In model-based shadow detection, a priori information about the 3-D geometry of the scene and the objects and the direction of the light source should be available [8]. There are some drawbacks, since additional input is required besides the image itself. A problem could be faced, if one does not have enough information about the light source and its position. However, for aerial images, if the date and time of the image are known, one could get solar angles calculated by some specific algorithms [http://www.nrc-cnrc.gc.ca]. Another drawback is that 3-D geometry information may not be available for every scene and even if it is available, it will be difficult to process shadows that belong to non rectangular shaped objects. These problems are also summarized in [4] and [8].

This class of shadow detection methods is not very common, since the additional information might not be always available. One of the rare examples is the method in [1], where Li et al. has used this approach by using an aerial input image and also a digital surface model (DSM) of the same scene and sun altitude at the relevant time.

3.2.2.2 Feature-based Shadow Detection

Feature-based shadow detection is more popular than model-based methods and there are several and different types of feature-based shadow detection methods in the literature [8].

In feature-based shadow detection, shadows are identified by using the properties of shadow, such as lower luminance.

In following sections, feature-based shadow detection approaches are mentioned.

3.2.2.2.1 Threshold-based Shadow Detection

The first type of feature-based shadow detection algorithms to be mentioned is threshold-based shadow detection. Threshold-based methods depend on

the shadow features that are analyzed in the previous section. Either a simple thresholding to the Value component in HSV color space (or equivalent component in similar color spaces) could be preferred as in [2], [28] or some other approach that includes other shadow features as well, also might be the choice [4], [34], [36], [36], [38], depending the input image properties and also accuracy and simplicity that is necessary for the performance.

3.2.2.2.2 Edge-based Shadow Detection

Shadow detection could also be achieved by detecting shadow edges. Shadow edges could be obtained by using an invariant color space or similarly using an illumination invariant image. The intrinsic images could be found by using methods like [27] or [30].

Salvador et al. [8] and Sarabandi et al. [9], used $C_1C_2C_3$ color space in order to detect the shadow edges. They claim that $C_1C_2C_3$ color space is invariant to shadow. The experiment above with the sample images, however, not fully agrees with this assumption. However, still this approach could be used and successful results could be obtained for some content, as shown in Figure 15 and Figure 16:

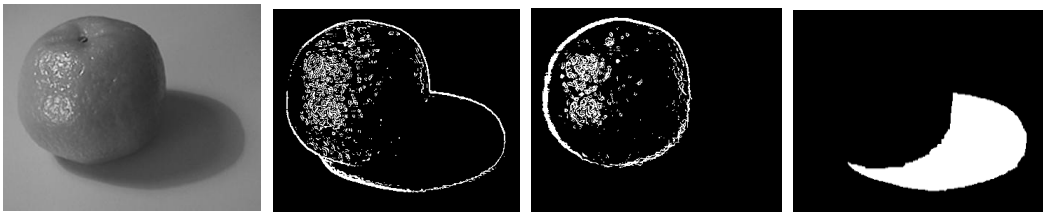

Figure 15 – The shadow detection result in [8], from left to right: original image, edge of object and shadow, edge of object, detected cast shadow

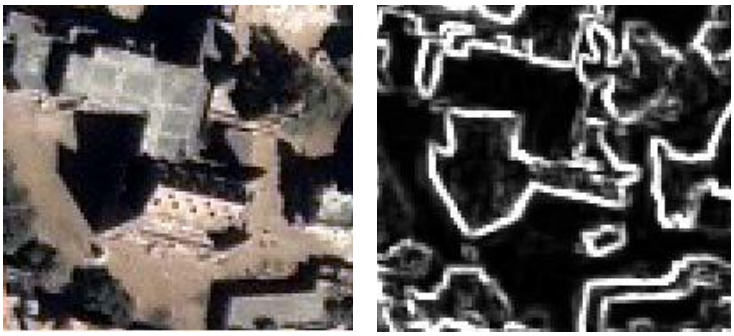

Figure 16 – The shadow detection result in [9]

Another approach for detecting edges could be as follows: First finding and illumination invariant image then by finding edges in both original and illumination invariant image and finally labeling the common edges as shadow boundaries. This approach is used in [10] and [29] by Finlayson et al. The experimental result in [29] is given below:

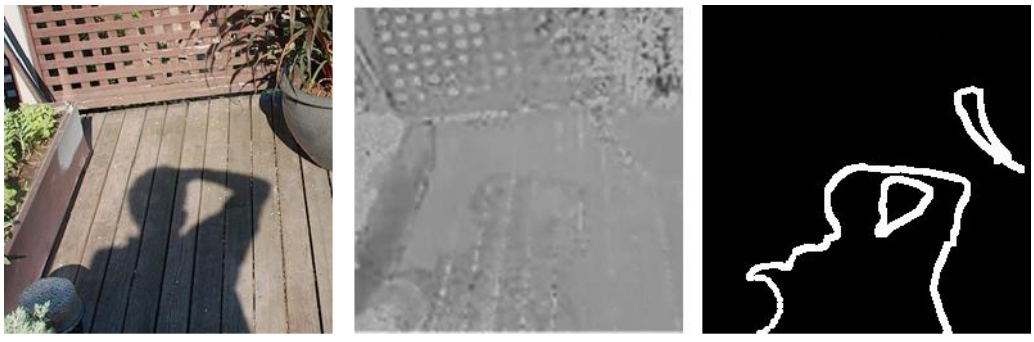

Figure 17 – Shadow detection result [29], left: original image, middle: illumination invariant image, right: detected shadow edges

Edge classification is preferred by Levine and Jisnu Bhattacharyya in [14]. They use Support Vector Machine (SVM) classifiers to classify the detected edges as shadow boundaries. Naturally, a training process is needed to utilize this approach, which will be accepted as user input to the process, during comparison with other algorithms that are fully automated.

Barnard and Finlayson [16] segmented the input image to the same color regions and then they labeled the boundaries of the regions as shadow edge if they hold the relevant feature for a shadow boundary.

3.2.2.2.3 Other Feature Based Shadow Detection Methods

There are some other methods, which will not fall into above classes. One example is Etemadnia and Alsharif's homomorphic approach for shadow detection defined in [3] where they filter the illumination component of the image in log domain to extract shadows.

Another example is given in [15] where Zhongfei and Zhang come up with a different method that uses expectation maximization algorithm on the image represented as graph. Other example studies that fall into this category are [39], [51], [52] and [53].

3.3 Compared Shadow Detection Methods

In this section, compared shadow detection methods are explained in detail.

Shadow detection could be done in several ways that change depending on the input image properties, its metadata availability, user input opportunity and similar case specific parameters.

Model based shadow detection could be a choice if we have the digital surface model of the scene and sun angles. The sun azimuth and elevation angles associated with an aerial or satellite image could be found if the date and time of the image taken. However the digital surface model for an arbitrary scene may not be available. So in this study, feature based shadow detection approaches are preferred to be compared. Among feature

based class of methods, some threshold based methods and a homomorphic based method is selected to be compared.

The threshold based shadow detection methods in the literature usually utilize the HSI/HSV color space components in order to detect shadows, since shadow regions shows distinctive features mostly on HSI/HSV color space, as discussed in the previous section. The thresholds could be selected by any thresholding technique, such as Otsu method [55] for any of the threshold based methods. The Otsu thresholding method is selected for this study since there is a direct implementation available in Matlab and it is simple to use.

When auto threshold is used, usually the whole sequence will be automatic, but in case where the user want to fine tune the threshold in order to get better results, a user input would be considered. Thus, manually suggested thresholds will also be mentioned for each approach.

3.3.1 (I-S) Difference Threshold Based Method [35]

Polodorio et al. [35] proposed a threshold based algorithm for aerial image shadow detection. They used the (I-S) difference of the components of HSI color space. Their approach uses the shadow feature that I values decrease and S values increase with shadow. Hence, (I-S) difference should be low for shadow regions and it will be high in non-shadow regions. The threshold could be selected as “0” for smaller distance sensors, such as airborne sensors or “-0.2” larger distance (orbital) sensors, such as Landsat TM or IKONOS [35]. This method is implemented as (S-V) in this study, in order to get a shadow mask parallel to the other methods, where we look always a higher value than a threshold for shadow.

3.3.2 NSVDI Threshold Based Method [4]

Another similar approach to (I-S) difference [35], is the “normalized saturation value difference index” (NSVDI) threshold based detection algorithm [4]. This work also deals with aerial images, like the ones in

Polodorio et al. [35]. It is shown in [4] that an improvement could be achieved to the performance of the previous (I-S) difference threshold approach of Polodorio et al. [35] by an example.

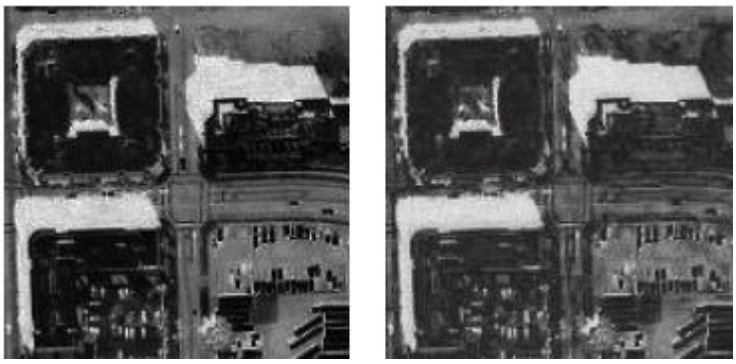

Figure 18 – The comparison of (I-S) difference image (on the left) and NSVDI ratio image (on the right) [4]

NSVDI is calculated for each pixel (i,j) in an image as below:

$$NSVDI_{(i,j)} = \frac{S_{(i,j)} - V_{(i,j)}}{S_{(i,j)} + V_{(i,j)}} \qquad (3.8)$$

A threshold “0” is experienced on an IKONOS image in the original study [4] and the shadow detection results seem successful.

3.3.3 Hue Threshold Based Method [36]

Huang et al. [36] proposes Hue threshold based method after mathematically showing that in shadow regions the Hue value increases. They define a 4 step approach where in the first step they segment the image into two by applying a threshold (T_1) to H component of the HSI color space. The first step shadow mask is given below denoted as S_c:

$$S_C = \{(i,j)|H(i,j) > T_1\} \qquad (3.9)$$

In this candidate shadow mask, it is mentioned [36] that there are also *bluish* regions, such as blue buildings, rivers, lakes etc. and *greenish* areas, like grasslands, where also higher hue values are observed. Bluish regions show high B values, while greenish regions show high G-B difference values [36]. Hence, in order to get rid of these false detections, the following two steps are required.

In the second and third steps, the bluish and greenish regions are removed from the high Hue valued segment. The bluish objects are removed by applying a threshold T_2 to B component, whereas the greenish objects are removed by applying another threshold T_3 to (G-B) difference, where B and G are the Blue and Green components of the RGB color space. The second and third step shadow masks are given below, respectively:

$$S_C{}' = S_C \cap \{(i,j)|B(i,j) > T_2\} \qquad (3.10)$$

$$S_C{}'' = S_C{}' \cap \{(i,j)|(G(i,j) - B(i,j)) > T_3\} \qquad (3.11)$$

The final step is the removal of small noisy regions from the shadow mask by applying morphological operators [36]. The morphological “opening” operation was applied to get rid of the small patches while a “closing” operation is applied to remove the small holes in the shadow mask.

The three threshold values are not given in the original work [36]; however, in a comparative study of Tsai [34], this approach is experimented with $T_1 = 0.1$, $T_2 = 80$ and $T_3 = 80$ threshold values in one image and $T_1 = 0.41$, $T_2 = 116$ and $T_3 = 70$ in another image mentioning that the values are selected manually with trial and error method.

3.3.4 (He+1) / (Ie+1) Ratio Threshold Based Method [34]

Tsai [34] proposed a method that is based on $(H_e+1) / (I_e+1)$ ratio threshold, where H_e is defined as hue equivalent and I_e is defined as intensity

equivalent components. H_e is selected as the H component in HSI, HSV and HCV color spaces, Q in YIQ color space and C_r in YC_bC_r color space. I_e is selected as the I component in HSI color space, V in HSV and HCV color spaces, Y in YIQ and YC_bC_r color spaces. The threshold is selected with Otsu [55] method but mentioning that a trade of exists between automating of the detection process and accuracy of the shadow detection [34].

Tsai [34] has experiment the Hue threshold based approach [36], (I-S) difference threshold approach [35] and a derivative version of (I-S) difference threshold approach that normalizes the (I-S), by comparing his own proposed method. His proposed method that uses HSI color space components gave superior results [34].

Similar to Huang et al. [36], Tsai [34] also has a final step that removes the potential false detections and noisy regions from the shadow mask. A Sobel operator is applied to the I_e component to get the gradient mask and then Otsu [55] threshold is applied to get a logical gradient mask. By eliminating the isolated holes with the morphological “closing” process, a shape mask is obtained. Then, finally, by using the “and” operator with this mask and shadow mask, a final shape preserved shadow mask is obtained.

3.3.5 Value Threshold Based Method [2], [28]

Beside these methods, simply a threshold to the grey value of the image could be a choice, since the best known feature of shadow is the decreasing intensity [2], [28]. The intensity equivalent component of any color space which is defined in [34] could be selected as grey value.

3.3.6 Novel Proposed Threshold Based Methods

Also other ratios could be used in which they depend on the shadow features. So novel ratios for shadow detection are also proposed and experimented in this thesis work.

These proposed ratios are (H+S+1)/(V+1), (H+S+1)/(V^2+V+1) and (S+1)/(V+1) where H,S and V are the components in HSV color space. For these ratios, the increasing values H and S are put over the decreasing V value in order to get a ratio value that increases in shadow regions. Similarly a threshold could be applied and the image will be segmented into shadow and non-shadow regions.

3.3.7 Homomorphic Based Method [3]

A different method to shadow detection which utilizes a homomorphic approach is Etemadnia and Alsharif's method in [3]. In their method, the image is first modeled as the multiplication of illumination and reflectance components [54]. Then, the illumination component is separated from reflectance component by knowing that the illumination changes are spatially varies slower than the reflectance component [3]. This step is achieved by applying a low pass filter to the V component of the HSV color space and then after getting the illumination part a threshold is applied and shadow mask is obtained. Below is the block diagram of the method [3] is given:

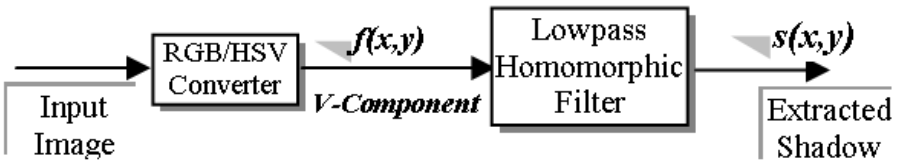

Figure 19 – Block diagram of the method [3]

3.4 Experimental Results

3.4.1 Comparison of Methods on Uniform Colored Sample Images

The values or ratio values in the threshold based methods in the literature and the proposed novel approaches are firstly tested on sample uniform colored images that are given in Figure 8, where we could observe (see figures from Figure 20 to Figure 25) the values change with shadow.

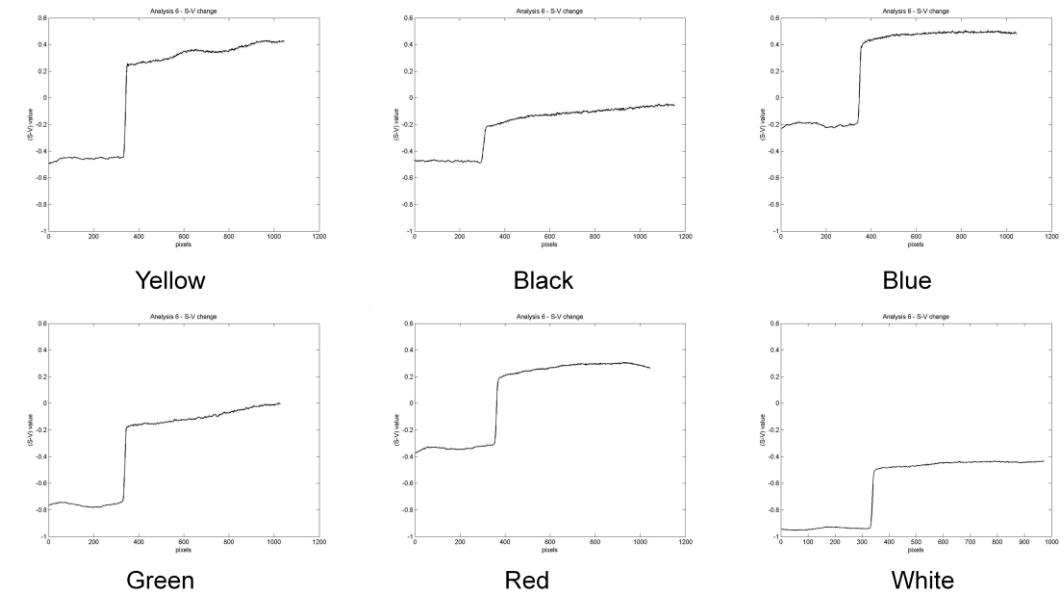

Figure 20 – (S-V) difference [35] change with shadow

As one could observe from Figure 20, (S-V) difference increases with shadow as expected. However, it is difficult to determine a single threshold for all the colors. Nevertheless, a threshold value of -0.1 could be an acceptable selection for these cases.

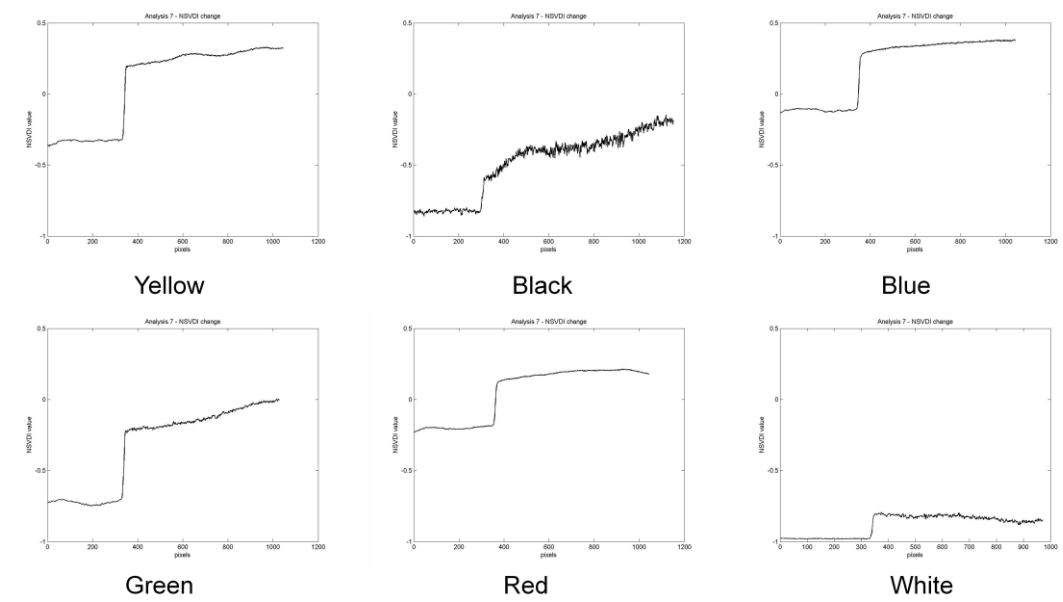

Figure 21 – NSVDI [4] ratio change with shadow

Similar to the (S-V) difference case, NSVDI measure also increases within shadow regions as expected. Similar to the previous (S-V) case, although a single threshold could not be determined for all the colors, a threshold value -0.1 would be a good selection for this case as well.

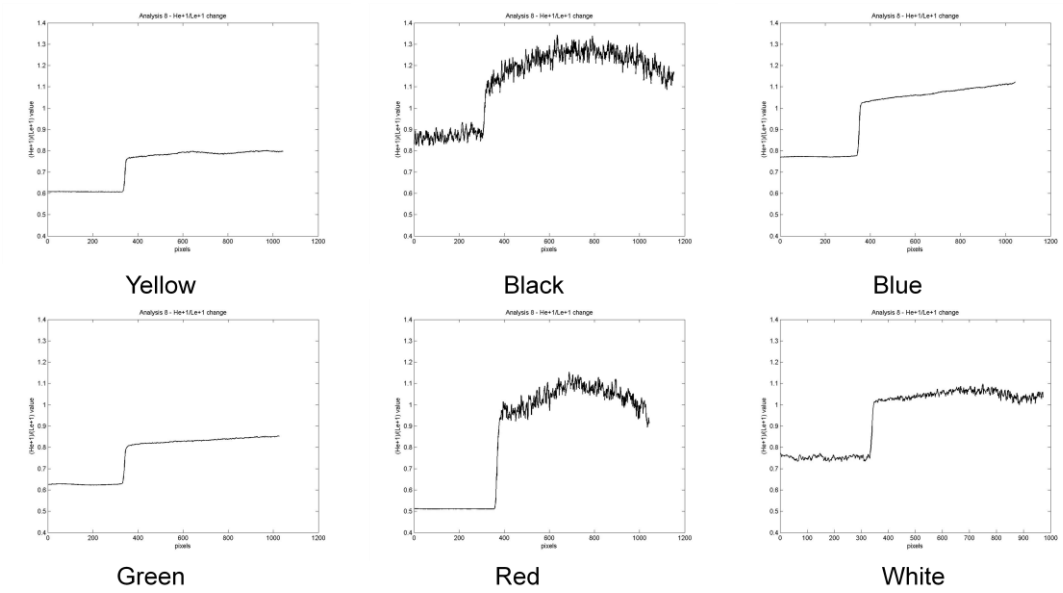

Figure 22 – (H_e+1) / (I_e+1) ratio [34] change with shadow

In most cases, (H_e+1) / (I_e+1) ratio increases within shadow region, except in black color. Since Hue also decreases in black color, where it is observed before in Figure 11, the ratio not increases but instead decreases. Hence, again a single threshold would not be determined to detect all the cases. However, a threshold value around 0.8 could be used to detect shadows.

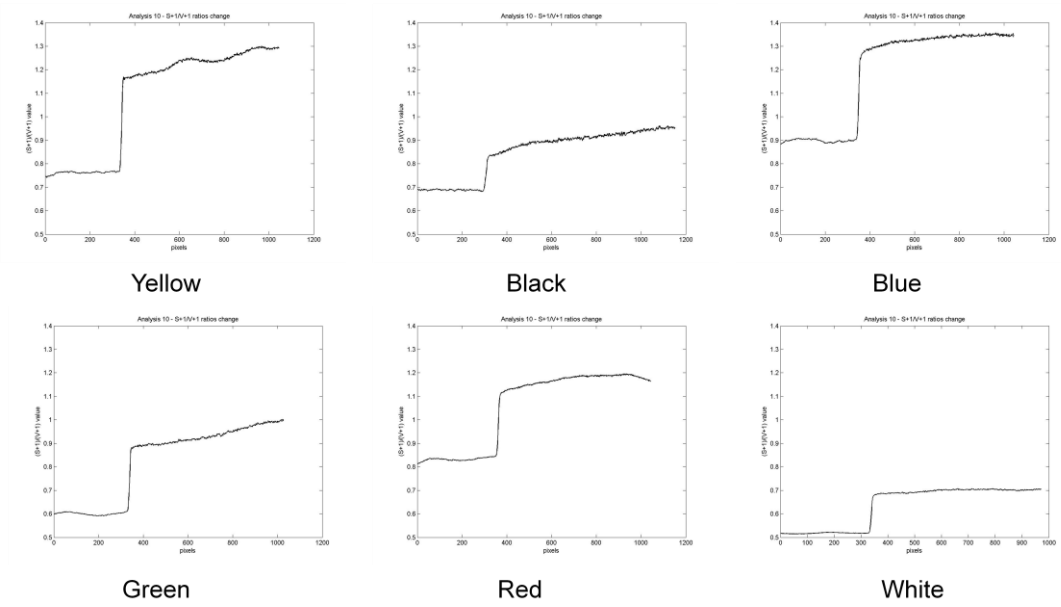

Figure 23 – (S+1) / (V+1) ratio with shadow

The results for the (S+1) / (V+1) ratio are similar to the (S-V) difference and NSVDI, since they all depend on S and V components. A threshold value 0.95 would be a reasonable selection for detection.

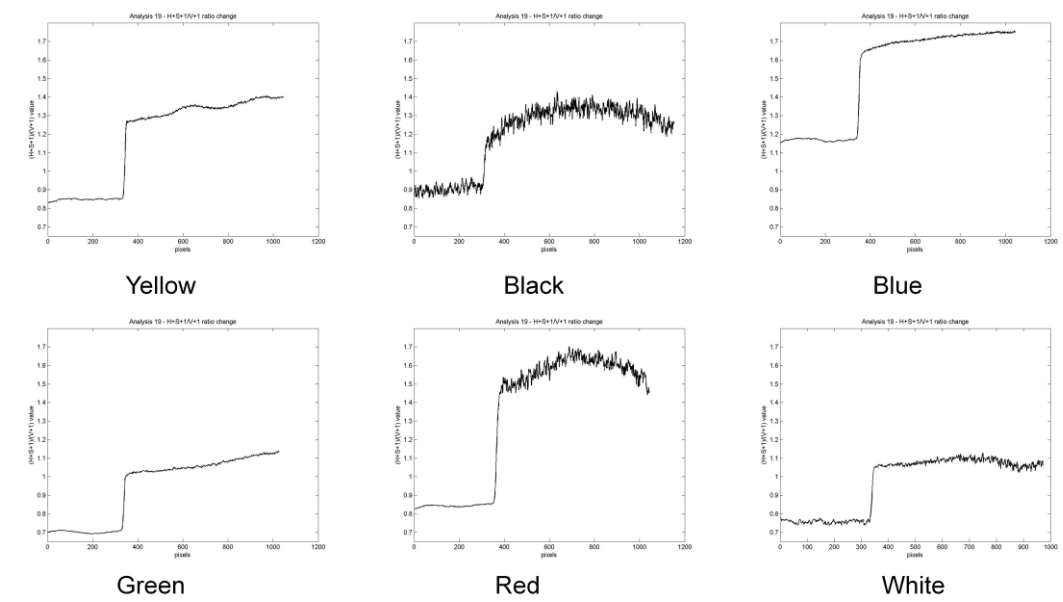

Figure 24 – (H+S+1) / (V+1) ratio change with shadow

The results in Figure 24 indicate that (H+S+1) / (V+1) ratio could be used to detect shadows except for blue color by using a threshold value of 1.

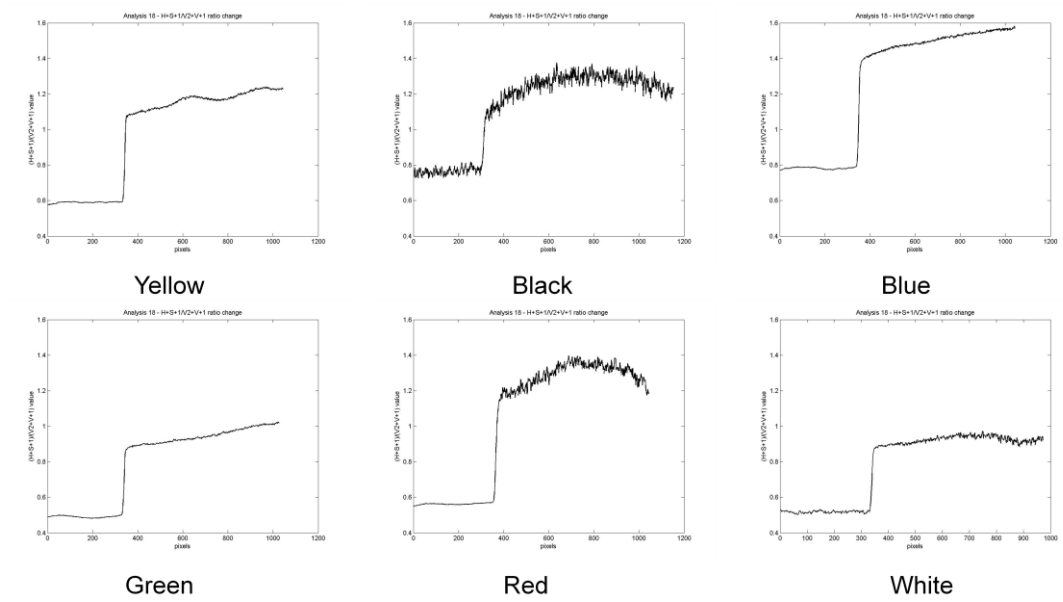

Figure 25 – (H+S+1) / (V^2+V+1) ratio change with shadow

The results in Figure 25 show that (H+S+1)/(V^2+V+1) ratio could also be used to detect shadows. A threshold with value 0.85 will be appropriate to detect shadows for all the sample colors.

Also a separation parameter calculation for the compared threshold based methods is proposed. This parameter is calculated from the difference of the non-shadow and shadow value of the method proposed. This parameter is referred as *separation value*. As seen from the table below, first method [35] and last method that novel proposed, have given better separation parameter values. However not only separation parameter value does not show methods performance but also a single threshold for all the colors could be set. As mentioned previously, a single threshold could not be set for the first method. However for the last method, a single threshold will be suitable for all the cases.

Table 1 – Separation parameter for shadow detection methods

	Yellow	Black	Blue	Green	Red	White	Average
S-V [35]	**0.79**	0.35	0.68	**0.65**	0.61	**0.49**	**0.60**
NSVDI [4]	0.57	0.44	0.45	0.58	0.39	0.15	0.43
(He+1)/(Ie+1) [34]	0.18	0.38	0.30	0.21	0.53	0.30	0.32
(S+1)/(V+1)	0.47	0.21	0.43	0.32	0.34	0.18	0.33
(H+S+1)/(V+1)	0.49	0.42	0.54	0.35	**0.75**	0.32	0.43
(H+S+1)/(V^2+V+1)	0.57	**0.51**	**0.71**	0.45	0.74	0.41	0.57

3.4.2 Comparison of Methods on a Sample Image with Ground Truth

Firstly, the methods are compared against an outdoor image with a manually obtained ground truth shadow mask.

The sample image and its ground truth shadow mask are given in Figure 26:

Figure 26 – Sample Shadowed Image and Ground Truth Shadow Mask

Figure 27 to Figure 31 illustrates the shadow detection results, where the accuracy of the method is denoted by AC. The accuracy is defined as the ratio of, the total number of true detected shadow and non-shadow pixels, to the total pixel number of the image [34].

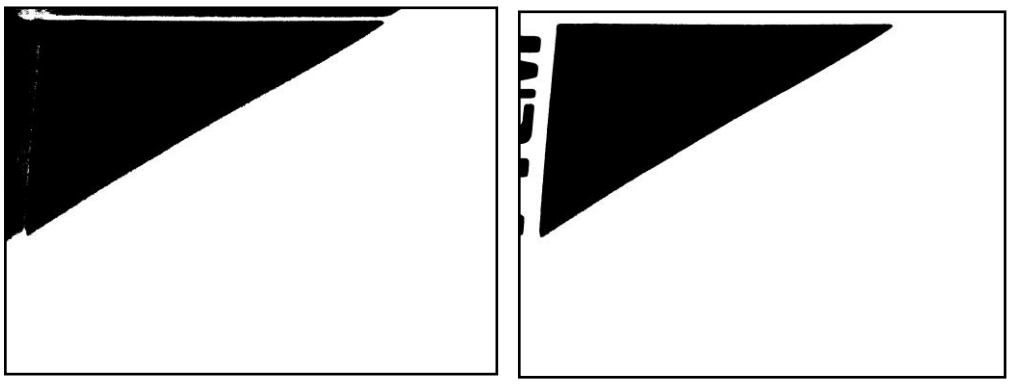

Figure 27 – Left: V threshold, AC = 98.8%; Right: (S-V) diff [35], AC = 94.8%

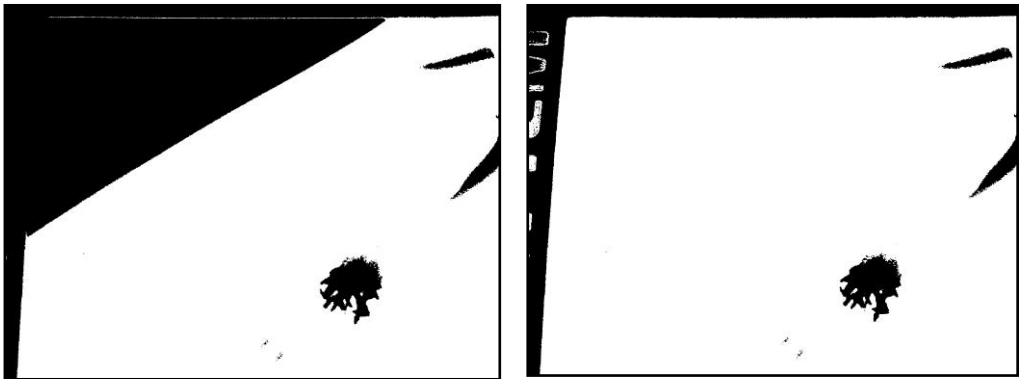

Figure 28 – Left: H threshold with bluish and greenish removal, AC = 96.0 %; Right: H threshold without bluish and greenish removal, AC = 75.3%, [36]

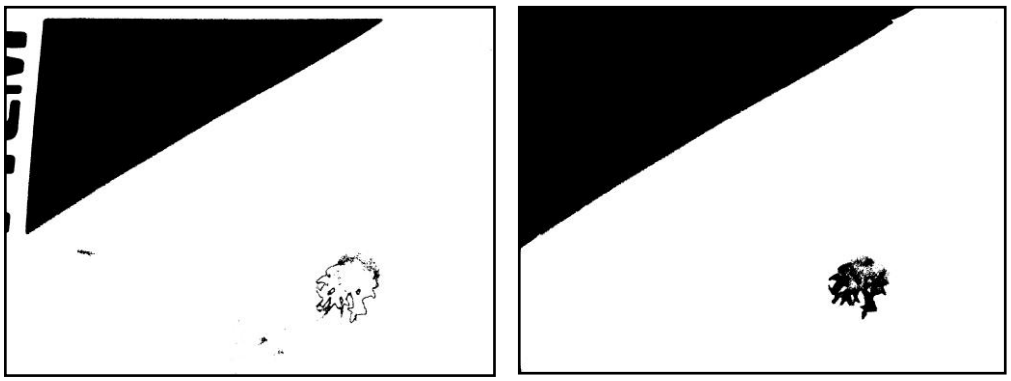

Figure 29 – Left: NSVDI threshold [4], AC = 94.4%; Right: $(H_e+1) / (I_e+1)$ ratio threshold [34], AC = 98.7%

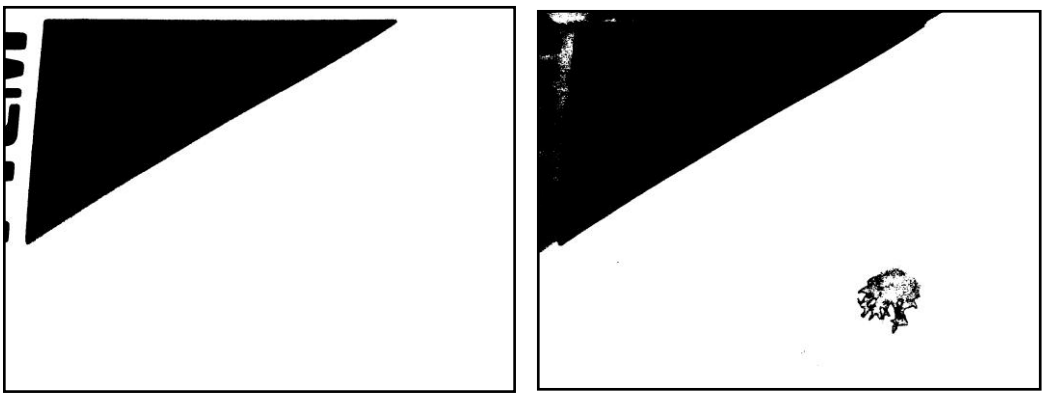

Figure 30 – Left: (S+1) / (V+1) threshold, AC = 94.9;
Right: (H+S+1) / (V+1) ratio threshold, AC = 98.8%

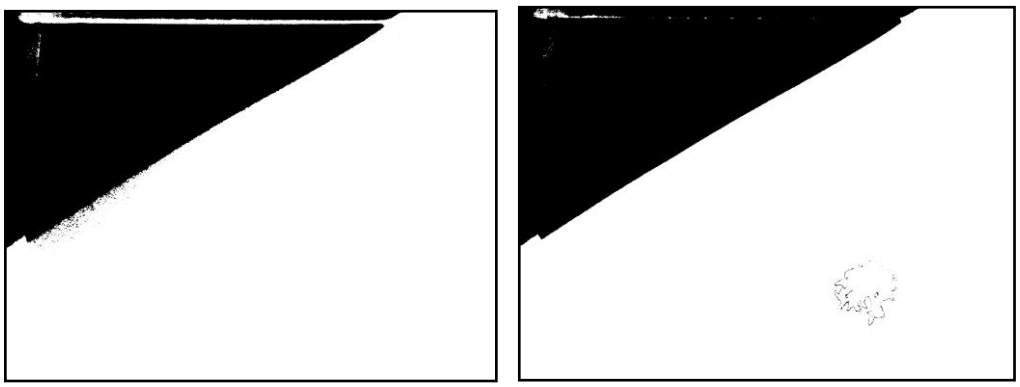

Figure 31 – Left: LPF based method [3], AC = 98.3%;
Right: (H+S+1) / (V^2+V+1) ratio threshold, AC = 99.5%

As it can be observed from the results between Figure 27 to Figure 31, (H+S+1)/(V2+V+1) ratio threshold gives the best results with 99.5% accuracy. The results of LPF based method [3], (He+1) / (Ie+1) ratio threshold based method [34], (H+S+1)/(V+1) ratio and simple V threshold are superior and the others are quite acceptable.

However, it should be noted that for every image the performance of each method could differ. In order to have an idea about the performance of the compared methods, some satellite input images are also used in the next section.

3.4.3 Comparison of Methods on Satellite Images

In this section, methods are compared on two satellite images. The first image, which contains some snowy regions, is selected to observe the performance of the methods in white regions that are covered by shadows which could be a hard task for detection methods. A second image, which includes some grassland and a pool, is selected in order to examine the effect of bluish and greenish removal step that is proposed in [36].

The first image and the results are given below. The shadow masks that are result of detections are given as blue overlaid on the original image instead of a shadow mask in order to easily observe the false detections.

Figure 32 – Sample Satellite Image 1

Figure 33 – (S+1)/(V+1) ratio based method with auto threshold

Figure 34 – H auto threshold with bluish and greenish removal method [36]

Figure 35 – H auto threshold without bluish and greenish removal method [36]

Figure 36 – (H+S+1) / (V+1) ratio based method with auto threshold

Figure 37 – (H_e+1) / (I_e+1) ratio based method with auto threshold [34]

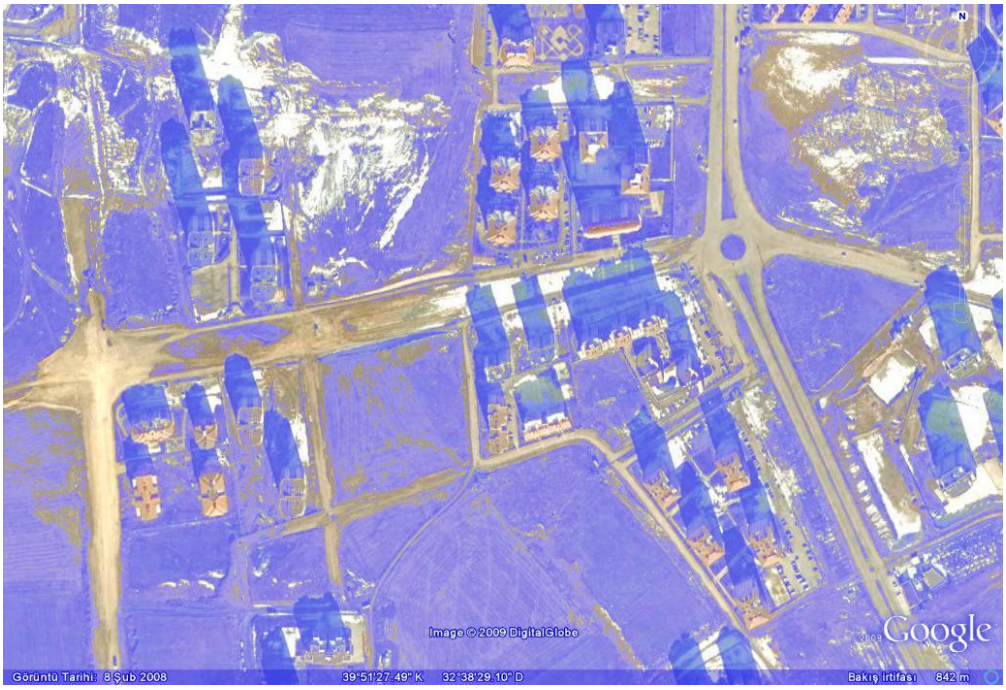

Figure 38 – LPF based method [3]

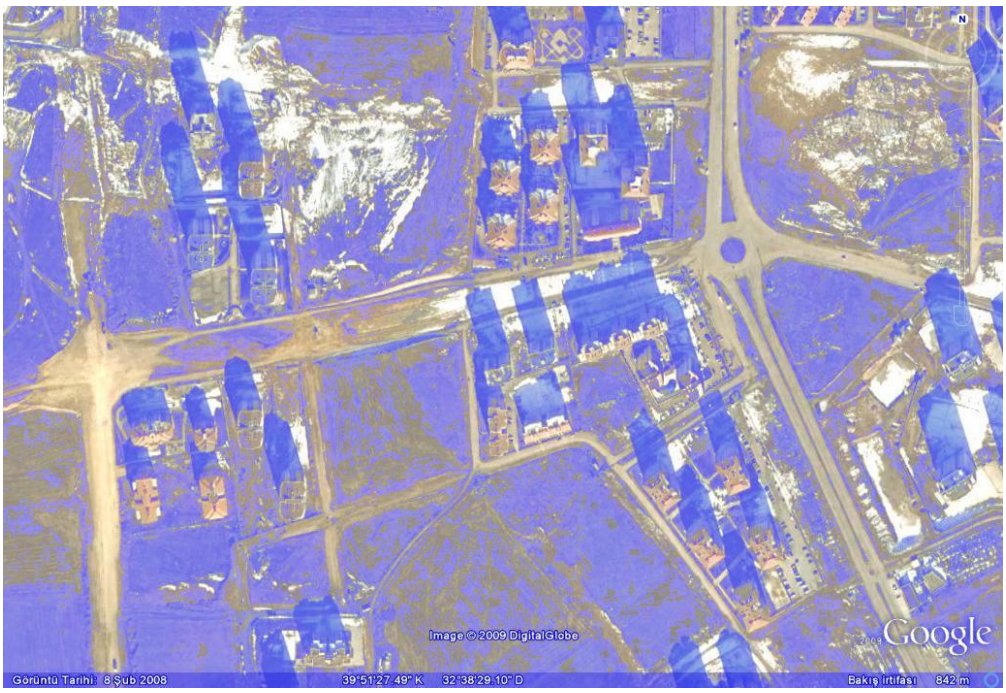

Figure 39 – (H+S+1)/(V^2+V+1) ratio based method with auto threshold

Figure 40 – (H+S+1)/(V^2+V+1) ratio based method with manual threshold = 0.8

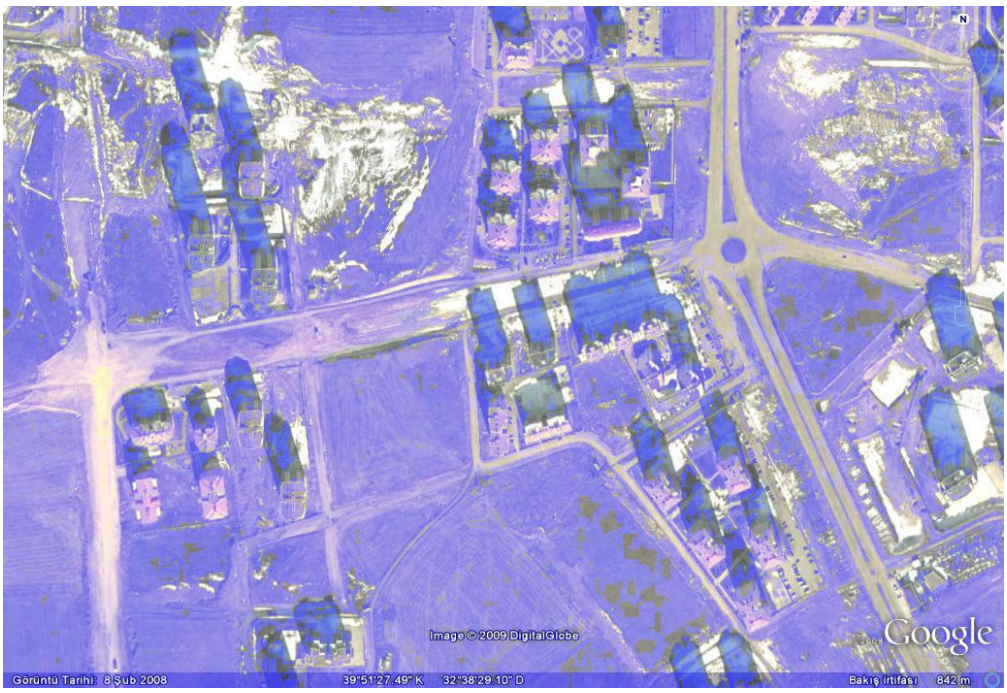

Figure 41 – NSVDI ratio based method with auto threshold [4]

Figure 42 – NSVDI ratio with manual threshold = 0 [4]

Figure 43 – NSVDI ratio with manual threshold = -0.2 [4]

Figure 44 – (S-V) difference based method with auto threshold [35]

Figure 45 – (S-V) difference based method with manual threshold = -0.2 [35]

Figure 46 – (S-V) difference based method with manual threshold = -0.3 [35]

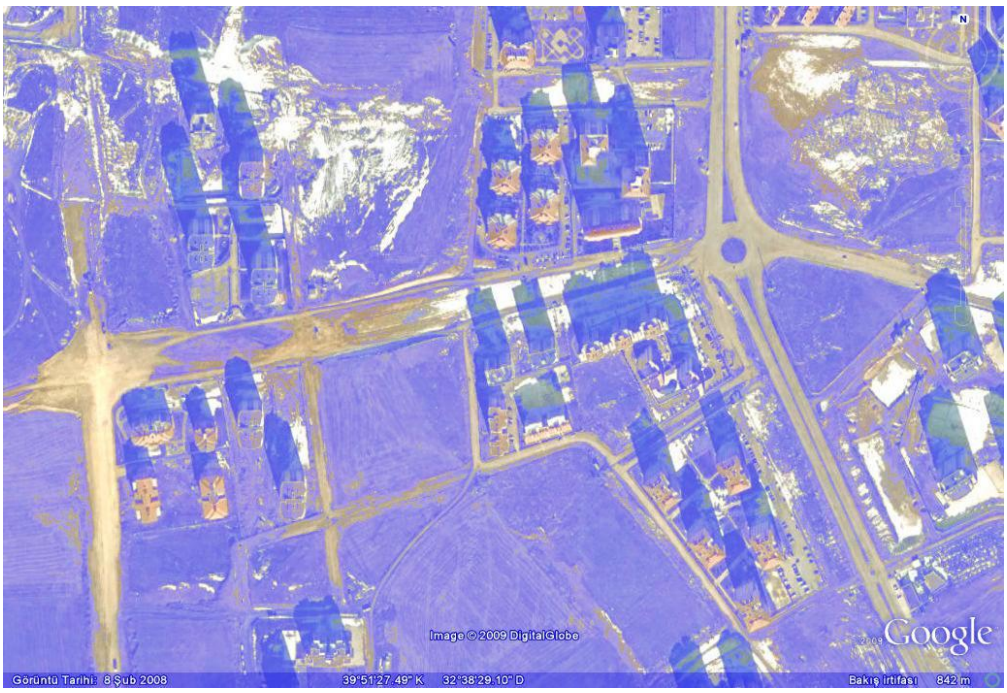

Figure 47 – V auto threshold based method

Figure 48 – V manual threshold = 0.45

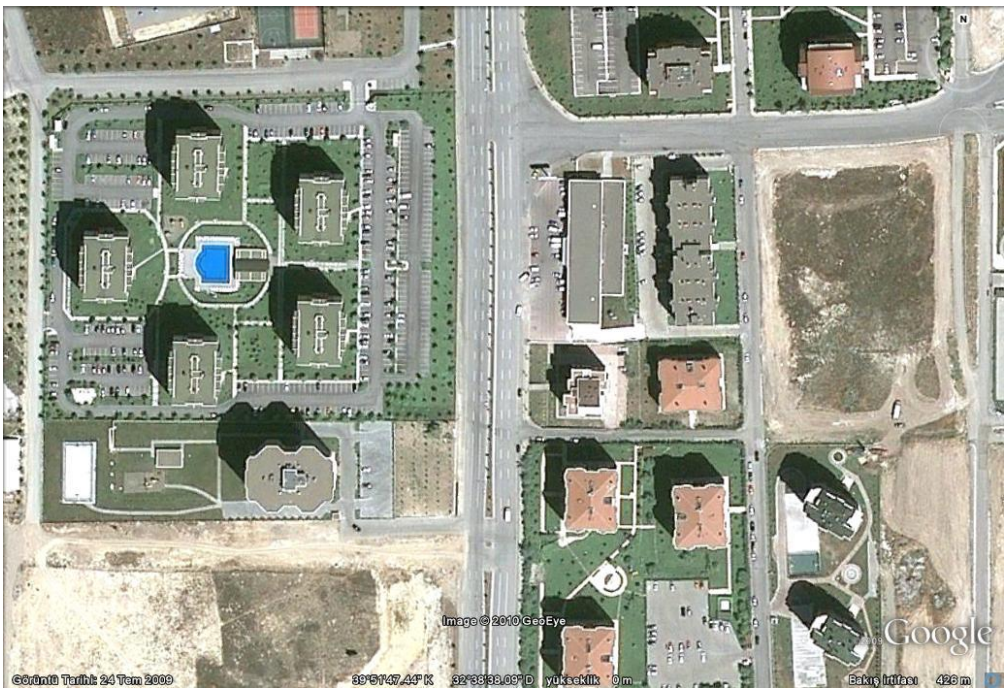

Figure 49 – Sample Satellite Image 2

Figure 50 – H auto threshold based method without bluish and greenish removal method [36]

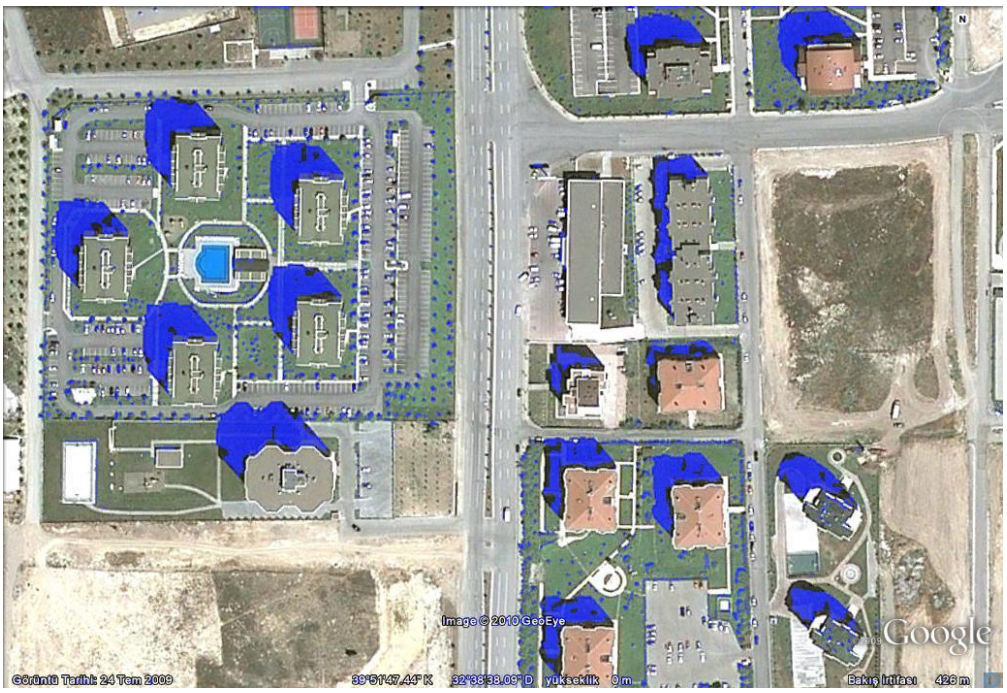

Figure 51 – H auto threshold based method with bluish and greenish removal method [36]

Figure 52 – (H+S+1) / (V^2+V+1) ratio with auto threshold

Figure 53 – NSVDI with manual threshold = 0 [4]

Figure 54 – (S-V) difference with manual threshold = -0.2 [35]

Figure 55 – NSVDI with auto threshold [4]

Figure 56 – NSVDI with auto threshold [4] combined with removal step of bluish and greenish regions [36]

Figure 57 – LPF based method [3] combined with removal of bluish and greenish regions [36]

Figure 58 – LPF based method [3]

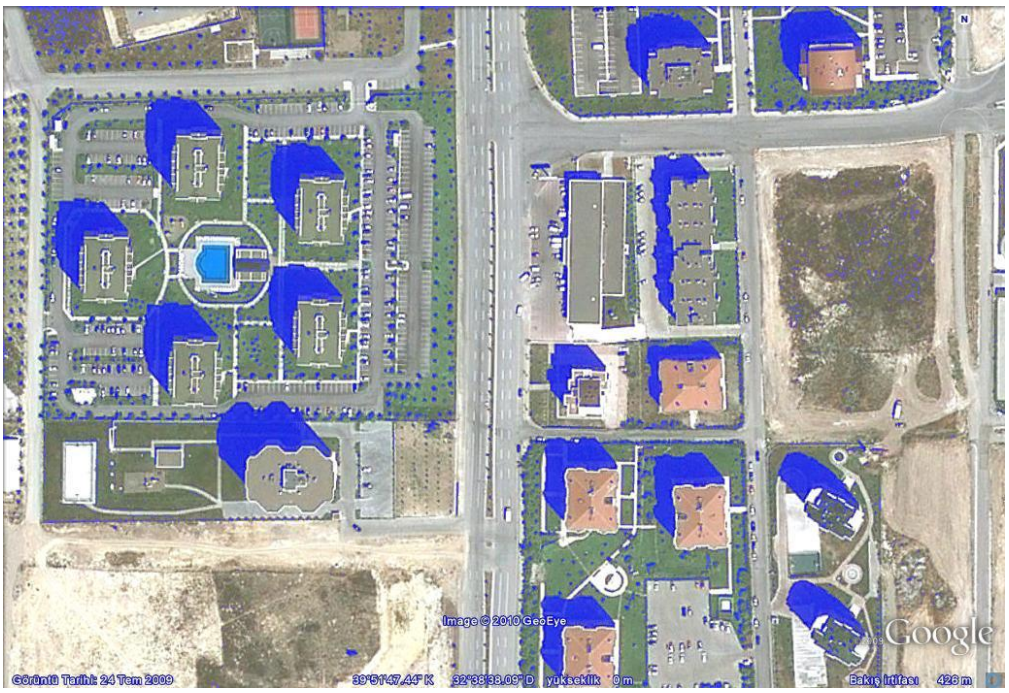

Figure 59 – (H+S+1) / (V+1) ratio auto threshold combined with removal of bluish and greenish regions [36]

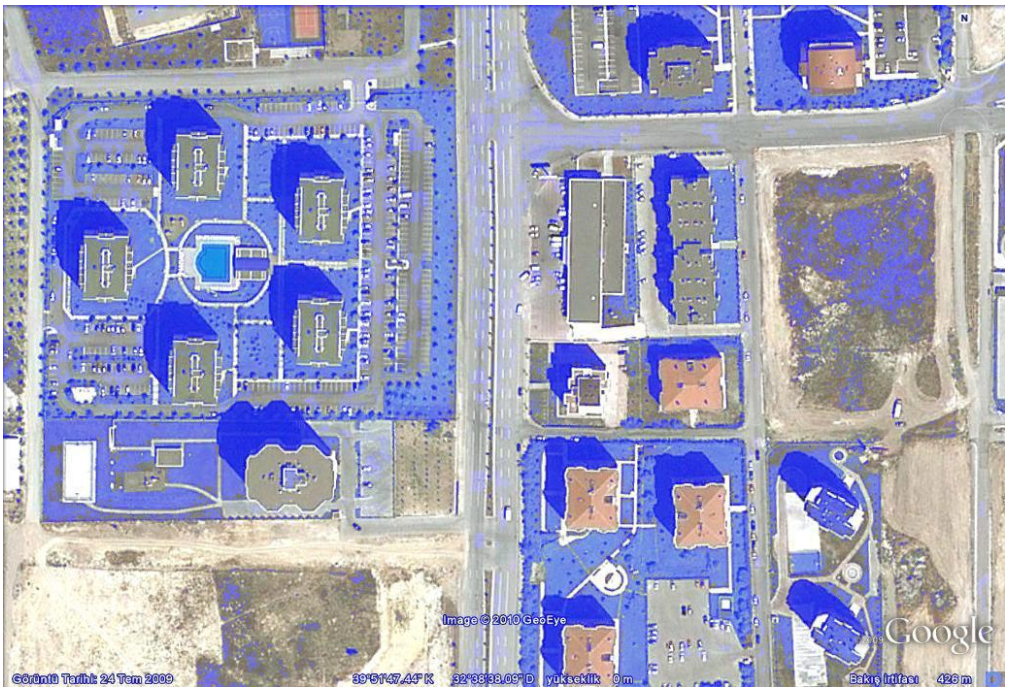

Figure 60 – (H+S+1) / (V+1) ratio (Otsu) threshold

Figure 61 – V auto threshold combined with removal of bluish and greenish regions [36]

Figure 62 – V auto threshold

Figure 63 – (H_e+1) / (I_e+1) ratio auto threshold method [34] combined with removal of bluish and greenish regions [36]

Figure 64 – (H_e+1) / (I_e+1) ratio (Otsu) threshold method [34]

3.5 Discussion about Shadow Detection Experimental Results

From the results between Figure 32 to Figure 64, one could observe that there is no single method that could be selected as leading approach. According to the observations, H threshold method with bluish and greenish removal step [36] provides good results.

The bluish and greenish removal step defined in [36] is also beneficial when combined with the LPF based detection [3], NSVDI threshold based method [4] (if threshold will be determined by Otsu method automatically), (H+S+1)/(V+1) threshold based detection, $(H_e+1)/(I_e+1)$ ratio threshold method [34] and V threshold method. Without this step, the detection results are unsatisfactory as seen in the shadow detection results for the sample image in Figure 50 and Figure 51.

However, $(H+S+1)/(V^2+V+1)$ ratio based method with a threshold selected as 0.8 provides superior results even without this bluish and greenish removal step. If the threshold is desired to be selected automatically and a small threshold value is calculated automatically, then unsatisfactory detection results could occur. The threshold was calculated 0.66 in the first image and 0.88 in the second image by Otsu method for $(H+S+1)/(V^2+V+1)$ ratio based method. From the experimental results, the automatic threshold value selected for this method may not be always appropriate. So a manual threshold around 0.8 will be a better choice when utilizing this method.

(S-V) difference threshold [35] based method provided good results for the second case but could not output satisfactory results on the first case. In case of NSVDI ratio [4] based method, the situation is the same as (S-V) difference threshold [35] based case. It is an expected results since it [4] is based on that [35] method. The LFP based [3] method did not output satisfactory results for both cases. But if the bluish and greenish removal step is added it could be observed that the detection result is better for the second case. The $(H_e+1)/(I_e+1)$ ratio threshold method [34] provided good

results for the first sample image but had problems with bluish and greenish areas in the second image. The output could be improved by adding bluish and greenish removal step to the process.

Eventually manual threshold in $(H+S+1)/(V^2+V+1)$ ratio based method and H threshold method with bluish and greenish removal step [36] provided good results for both cases.

CHAPTER 4

SHADOW COMPENSATION

The shadow compensation (or restoration) could be defined as restoring the texture of the shadowed region in order to obtain the same region with no shadow on it. Since shadows destruct the scene region under, they might degrade performance of some tasks, such as target detection, object recognition or image segmentation. Hence, shadow compensation is certainly a necessary intermediate step for such tasks in order to eliminate the undesired effects of shadow.

4.1. Overview of Shadow Compensation Methods

There are several types of shadow compensation methods. One class of compensation methods is based on direct removal of shadows without using a prior shadow detection step. Other class of compensation methods requires an input shadow mask that results from a shadow detection process.

Contrast enhancement could be used as a method for direct shadow compensation, since it does not require a detection step. A similar approach is given in [13], where image is partitioned to small blocks and processed. Firstly, the image is partitioned to square blocks and then by using the mean values of each block, the median of all these mean values are obtained. Finally, all the elements of blocks that their means are below the median are scaled with the estimated median value [13]. After this process, the shadows are eliminated from the image. This method is relatively simple and old method published in 1990 that works only on grey scaled images. A typical experimental result is given below [13]:

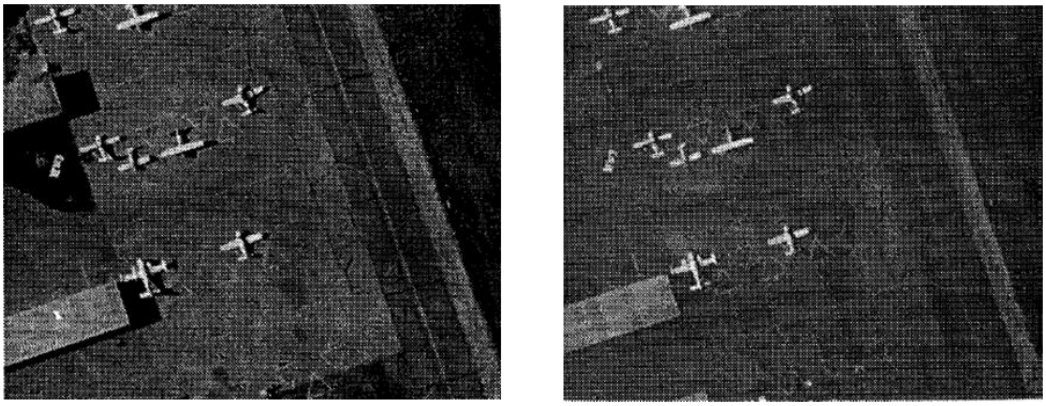

Figure 65 – Input image on the left, whereas output image on the right [13]

As it can be observed from the figure above, the result of the method in [13] for the sample image is not very satisfactory. For example, the upper left building has disappeared completely as a result of compensation. However, considering the simplicity of this method, this type of a distortion in the compensated image is expected, since there is no detection step that distinct shadow regions from the foreground objects.

There are also some other complex approaches proposed. An example for such methods is presented in [32], where a color image is used for compensation. The process is achieved in HSI color space. After conversion to HSI color space, I and S components are compensated separately and then combined again and converted back to the RGB image. H component is not changed during the whole process. Since the approach is probabilistic and depends on posteriori probability a training step is needed before the compensation process could be executed. Below the block diagram of the process is given [32]:

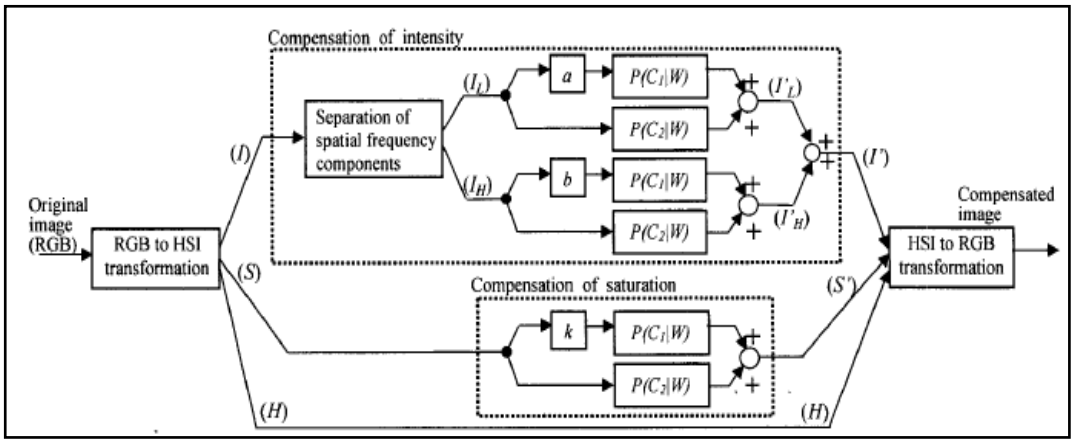

Figure 66 – Block diagram of the shadow compensation process in [32]

In the figure above, W represents the RGB color space components, C_1 is shadow class and C_2 is non-shadow class. The intensity component is first divided into high frequency and low frequency component and separately compensated. The low frequency and high frequency intensity components are scaled with different coefficients and weighted with posteriori probabilities. The scale values are greater than one that increases shadow pixels' intensities. On the other hand, the saturation component is also scaled and weighted with posteriori probabilities. However, the scale value is smaller than one that decreases the saturation value. The coefficients are selected in a heuristic manner and the reason for separating intensity components is to be able to use different coefficients for these.

Another class of shadow compensation methods is based on histogram matching. Histogram matching based approaches are preferred for shadow compensation in [4], [9], [28], [34] and [48]. Histogram matching based shadow compensation is defined in detail in the next section.

Gamma correction and linear correlation is also considered a different approach to shadow compensation by Sarabandi et al. [9] in addition to

histogram matching. These two methods are also defined in detail in the next section.

If more than one image of the same scene is available then multi-source data fusion [26], [28] could also be an option for compensating shadows.

On the other hand, edge based shadow compensation [7], [10], [29], [31], companion area intensity mapping [1], Retinex theory based compensation [36] and even just directly replacing the shadow pixels by its neighbor pixels [14] are other approaches for shadow compensation. Neural network based shadow compensation based approach is proposed in [33].

4.2. Compared Shadow Compensation Methods

In this study, some shadow compensation methods are examined through simulations. There are five methods that are implemented and tested on sample images [48], [34], [4], [9]. The first approach is global histogram matching on V component [48], whereas the second one is local histogram matching on V component where a shadow buffer zone is selected for the process for each connected shadow region [34]. In addition to these two methods, local histogram matching on all color components [4] is also tested. Beside the histogram matching, gamma correction and linear correlation [9] are also implemented as two different methods and tested on sample images. These methods are defined in detail below:

4.2.1. Histogram Matching Based Shadow Compensation

Histogram matching is defined as a process that produces an output image from an input image by matching its histogram to a specified one [54]. In histogram matching, we should map input grey levels to new grey levels. This could be done by taking the cumulative histograms of the original image and the specified histogram. Then for each input grey level find the output grey level that satisfies following equation:

$$F_{in}(\mathrm{x}) = F_{out}(\mathrm{y}) \qquad (4.1)$$

where F_{in} and F_{out} represents the input and output cumulative histogram functions respectively, x represents the input grey level and y represents the output grey level [34], [54]. In discrete case an exact equal case may not be found, instead the output grey value that minimizes the difference between cumulative histogram values is selected. In Figure 67 this process is depicted graphically, where shadowed region is the input and it is aimed to match the histogram of the shadow buffer zone. It depicts a shadow region pixel that has a gray value of 85 will be changed to 130 which is the corresponding grey level in the related shadow buffer zone [34].

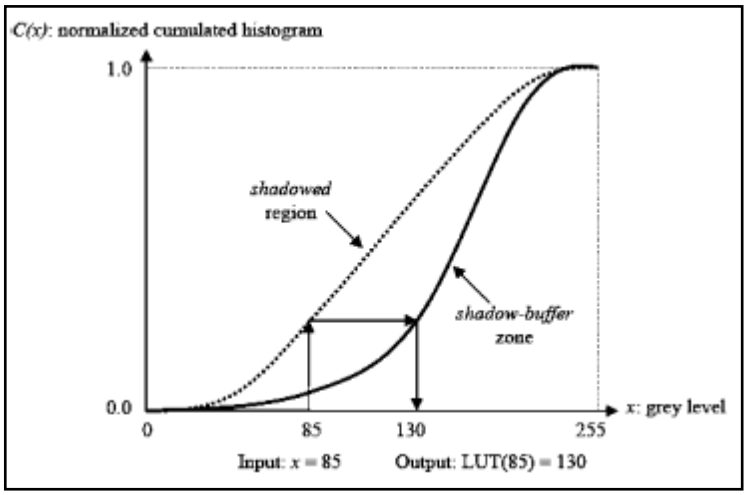

Figure 67 – Look up table (LUT) based shadow compensation process in [34]

4.2.1.1. Global Histogram Matching Based Shadow Compensation on V component [48]

Histogram matching could be applied to whole image as follows: All the shadow regions could be selected as input and it is aimed to match this input histogram to the histogram of the non-shadowed regions of the same image [48].

4.2.1.2. Local Histogram Matching Based Shadow Compensation on V component [9], [34]

For shadow compensation, a local histogram matching should be better than applying a matching in global image level, since the image radiometry could differ considerably for the whole image [28]. But this assumption is valid if the shadow regions not cover large portions of the image.

Hence, it is better to apply a histogram matching between shadow and non-shadow areas for the similar regions. Ma et al. [4] and Sarabandi et al. [9] referred selecting shadow and non-shadow areas that belong to the same class for histogram matching, but they did not mentioned how to determine the same class regions, which is a key step for this approach. However, selecting neighbor area of a shadow region could be a possible solution for this problem. Dare [28] and Tsai [34] preferred using neighboring regions for local histogram matching.

Tsai [34] proposed an approach consisting of two steps. In the first step, morphological operations are applied to the image to get a corresponding buffer zone of a connected shadow region. In the second step, histogram matching between this buffer area and connected shadow region is achieved and this process is applied for all the connected shadow regions for the whole image [34]. In this experiment the buffer width is taken as 10 pixels. This value is determined qualitatively by trial and error method on sample images.

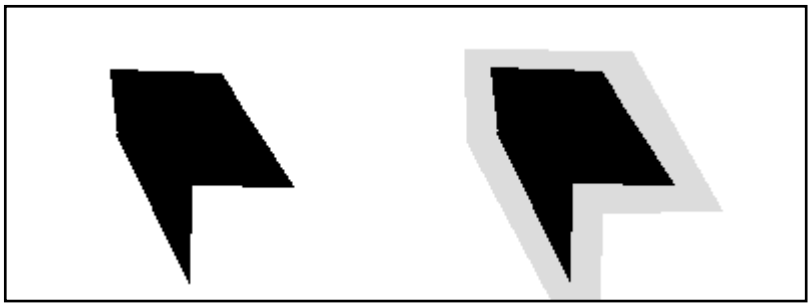

Figure 68 – An example connected shadow region (black) and its related buffer zone (grey)

4.2.1.3. Local Histogram Matching Based Shadow Compensation on H, S and V components [4]

In histogram matching, not only the intensity could be selected to adjust the luminance of the shadow region but also all the components of HSV color space could be chosen for compensation. While in [9], [34] and [48], only the intensity is compensated, in [4] all the HSV color space components of are compensated separately.

4.2.2. Gamma Correction Based Shadow Compensation [9]

Many image capture, printing and display devices has an exponential response. This exponent is called gamma value. For example cathode ray tube (CRT) display devices generally have a gamma value changing from 1.8 to 2.5. So these display devices generate a display, darker then compared to their input. In Figure 69 a plot is given to show this effect for different gamma values. For compensating this effect, a correction is done to the input generally at the source. The compensation is simply taking the exponentiation of input with a value of reverse gamma value. This process is called gamma correction.

Gamma correction with values greater than 1 has an effect on the image to make it brighter. So gamma correction could be considered as an alternative method for shadow compensation process [9].

$$\mathrm{V}_{recovered} = \mathrm{V}_{shadow}{}^{\frac{1}{\gamma}} \qquad (4.2)$$

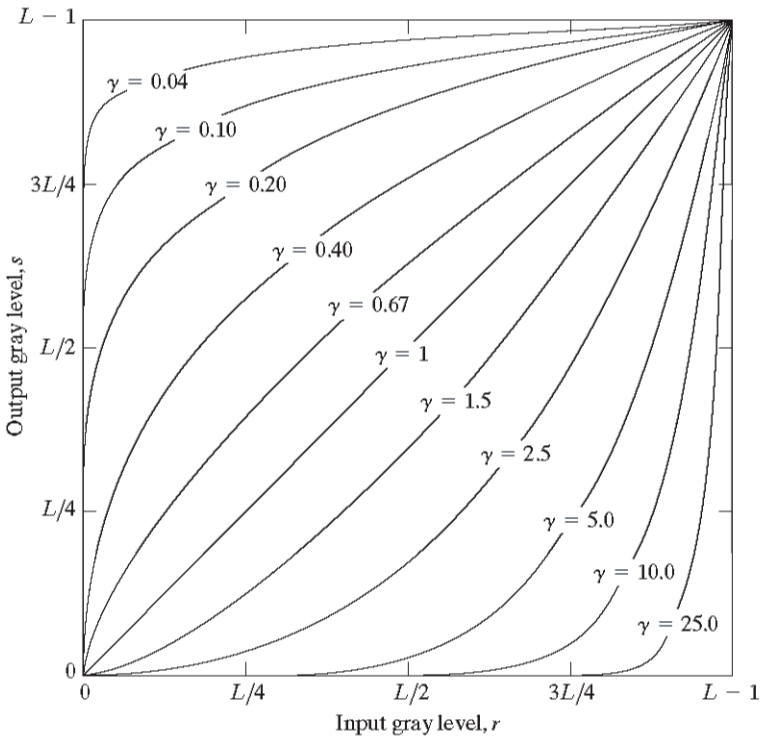

Figure 69 – Plots of output gray level for different gamma values

Sarabandi et al. [9] mentioned applying gamma correction between shadow and non-shadow regions of the same class of surfaces. In (4.1) the gamma correction formula is given where γ parameter is determined from the training data set [9].

Since finding same class of surface types are not so simple, in this experiment gamma correction is applied to a shadow region and its buffer zone [34]. The gamma value is taken as constant having a value 3 for all the cases. This value is found by qualitative trial method.

4.2.3. Linear Correlation Based Shadow Compensation [9]

Apart from gamma correction, linear correlation is also referred by Sarabandi et al. for shadow compensation [9]. Similarly, a shadow region and its neighbor pixels are selected and their mean value and standard deviations of are calculated.

$$V_{recovered} = \left(\frac{\sigma_{non-shad}}{\sigma_{shadow}}\right).(V_{shadow} - \mu_{shadow}) + \mu_{non-shad} \quad (4.3)$$

After this step, the process defined in (4.2) is applied to bring the mean and standard deviation of shadow regions to the related non-shadow region. Sarabandi et al. referred selecting this related non-shadow region by selecting the same class of surfaces. But similar to gamma correction case, in this experiment linear correlation is applied to a shadow region by using the mean and standard deviation values of its buffer zone [34].

4.3. Experimental Results

Three sample images are used. The first one is a satellite image of a region in Ankara-Cayyolu where high buildings are resulting shadows. The second one is also a satellite image of a region in Ankara-Cankaya. The last sample is an outdoor image bazaar street in Kirikkale.

The intermediate shadow detection step output, i.e. the shadow mask, is given as blue overlay over the original images.

Figure 70 – Sample image 1 for shadow compensation

Figure 71 – Shadow detection result for sample image 1

Figure 72 – Global histogram matching on sample image 1 [48]

Figure 73 – Local hist. eq. for V component on sample image 1 [34]

Figure 74 – Local hist. eq. for H,S and V components on sample image 1 [4]

Figure 75 – Gamma correction with parameter 3 on sample image 1 [9]

Figure 76 – Linear correlation based shadow detection on sample image 1 [9]

Figure 77 – An unsatisfactory shadow detection result for sample image 1

Figure 78 – Global histogram matching applied on unsatisfactory shadow detection for sample image 1

Figure 79 - Local histogram matching on H, S and V, applied on unsatisfactory shadow detection for sample image 1

Figure 80 – Sample image 2 for shadow compensation

Figure 81 – Shadow detection result for sample image 2

Figure 82 – Global histogram matching on sample image 2 [48]

Figure 83 – Local hist. eq. for V component on sample image 2 [34]

Figure 84 – Local hist. eq.for H,S and V components on sample image 1 [4]

Figure 85 – Gamma correction with parameter 3 on sample image 2 [9]

Figure 86 – Linear correlation based shadow detection on sample image 2 [9]

Figure 87 – Sample image 1 for shadow compensation

Figure 88 – Shadow detection result for sample image 3

Figure 89 – Global histogram matching on sample image 3 [48]

Figure 90 – Local hist. eq. for V component on sample image 3 [34]

Figure 91 – Local hist. eq. for H,S and V components on sample image 3 [4]

Figure 92 – Gamma correction with parameter 3 on sample image 3 [9]

Figure 93 – Linear correlation based shadow detection on sample image 3 [9]

Besides the shadow compensation comparison of the experimented methods, the time required to execute each compensation method is also compared. The execution time is given in Table 2. Also the dimensions and number of connected shadow regions of the sample images is given in Table 3.

Table 2 – Comparison of execution times of each compensation

Duration (seconds)	Image 1	Image 2	Image 3
Global HM [48]	1.5	1.9	1.3
Local HM on V [34]	5.6	33.8	6.6
Local HM on H,S,V [4]	10.6	68.0	13.0
Gamma correction [9]	3.5	20.6	4.1
Linear correlation [9]	5.3	35.2	6.2

Table 3 – Dimensions of sample images

	Image 1	Image 2	Image 3
Dimensions (pixels)	918x575 (527850)	1032x703 (725496)	800x600 (480000)
Connected shadow region numbers	18	109	25

4.4. Discussion about Shadow Compensation Results

Based on the experimental results, it could be concluded that none of the methods achieved completely neutralization of the shadow effect. However, it can also be qualitatively stated that the local histogram matching on H, S and V components had better results than the other methods. Gamma correction based shadow compensation, usually gives not very satisfactory results. One other drawback of this method is the requirement to determine a gamma parameter input to the process. Sarabandi et al. mentioned using a training step to determine gamma parameter [9], but during the experiments, the gamma value is taken as 3. This value is determined manually by trial and error method.

One another conclusion is that local histogram matching leads better results than global histogram matching. Linear correlation method performance is similar to global histogram matching.

If only the V component is compensated, then a blue cast is usually observed as a result of the Rayleigh scattering effect. This is also mentioned by Suzuki et al. in [32].

Hence, it can be stated that, local histogram matching on H, S and V components could be selected for shadow compensation. However, there is also another metric obtained during the experiments: execution times for each method. This metric gives an indication of the computational complexity for each method. From Table 2, it could be observed that our preferred method [4] requires more execution time compared to that of the other methods. It could also be observed that global histogram matching needs considerably less time than the other methods. Considering that this method [48], could also gives acceptable results for some scenes, such as sample image 1 and 3, it could also be preferred, if the processing time is an important issue. As it can be observed from the Table 2, except for the global histogram matching, the execution time changes depending on the image. However, this execution time change depends on the number of

connected shadow regions, more than the image size, as seen from Table 2 and Table 3. For example, even the image size of sample image 3 is smaller than the sample image 1, duration for image 3 is more than the image 1 for local histogram matching, gamma correction and linear correlation methods.

The duration of the local processed methods could be decreased by tying to minimize the connected shadow region number. This could be achieved by applying a filter or morphological operators to the shadow mask. Removing small regions of shadows from the shadow mask would also help to minimize the number of the regions.

The overall shadow compensation process performance depends not only to the selected compensation method but also to the initial shadow detection result. As it can be observed from Figure 78 and Figure 79, an unsatisfactory detection result will also lead to an unsatisfactory shadow compensation result. So for the shadow compensation process the prior necessary step is a shadow mask that is detected precisely.

Eventually, the method selection for shadow compensation will depend on the priorities. If execution time of the process is more important than the compensation result, then global histogram matching method could be selected. However, if execution time is not very important, then local histogram matching on H, S and V could be a better choice by considering minimizing the number of the connected shadow region methods

CHAPTER 5

BUILDING HEIGHT ESTIMATION: APPLICATION OF SHADOW ANALYSIS

An application of area of shadow analysis is building height estimation in aerial images [44], [45], [46], [56], [57]. Buildings typically occlude the sun light in the opposite direction of the sun azimuth angle, hence, this situation results cast shadows beside them. Using this shadow length, as well as satellite and sun angles information, one could estimate a buildings height.

5.1 Overview of Building Height Estimation Methods

There are usually two fundamental steps in building height estimation from shadow analysis. Firstly, the shadow length is extracted. Then, as a second step, the building height is calculated by using this data in addition to satellite and sun angles.

Shadow length could be calculated as a distance from a detected corner to the related shadow corner. However, relating the corners may not be simple and also taking just one sample line might lead to errors; hence, other approaches should be exploited searched. A robust method is defined by Kim et al [57].

In this part, shadow length calculation method is explained from the method in [57], where the shadow mask and projected shadow matching are achieved by finding the saturation point of the pixels in the overlapped region. Beside this approach, another approach could be pursued, where the projected shadow region’s pixels are examined with original shadow

region in terms of non overlapping pixels. Hence, as soon as the error starts to increase, the algorithm stops tracing the shadow region. This approach is depicted in Figure 94.

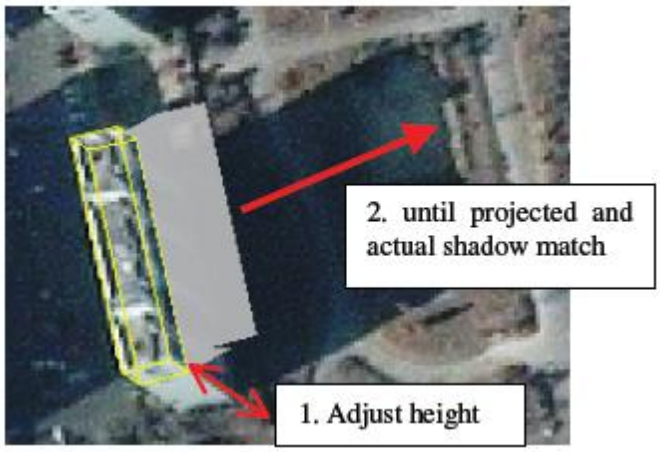

Figure 94 – Shadow projection method depiction in [57]

After this process using shadow length, sun angles and satellite angles the building height could be calculated. In [56] and [44], the height estimation formula is given for the general case. However, in [45], the extraction is obtained only when the sun and satellite azimuth angles are equal to each other.

Below a geometrical depiction of a building and its cast shadow related with sun and satellite angels are given:

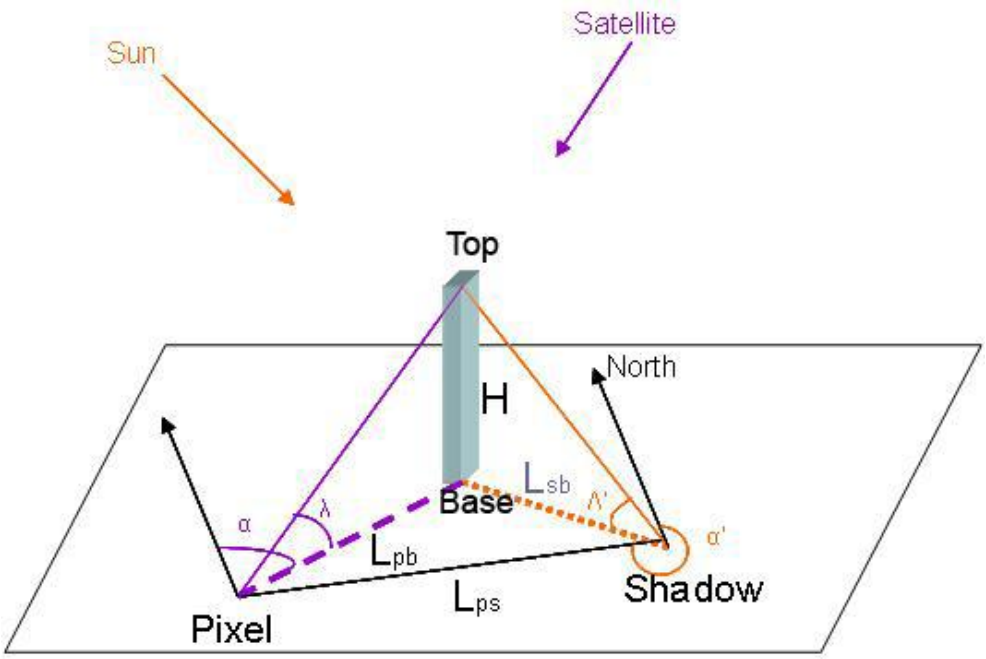

Figure 95 – Geometrical depiction of a building and its shadow [56]

In order to derive the building height from this geometry, the following steps are followed. Firstly, the following three equations are derived from the related triangles.

$$H = \tan\lambda . L_{pb} \qquad (5.1)$$

$$H = \tan\lambda' . L_{sb} \qquad (5.2)$$

$$L_{ps}{}^2 = L_{sb}{}^2 + L_{pb}{}^2 - 2 . L_{pb} . L_{sb} \cos(\alpha - \alpha') \qquad (5.3)$$

By using these three equations the building height H can be calculated as follows:

$$H = \frac{L_{ps}}{\sqrt{\left(\frac{1}{\tan^2\lambda'} + \frac{1}{\tan^2\lambda} - \frac{2 . \cos(\alpha - \alpha')}{\tan\lambda' . \tan\lambda}\right)}} \qquad (5.4)$$

where α and λ represents the satellite azimuth and elevation angles and α' and λ' represents the sun azimuth and elevation angles respectively.

In case of sun and satellite azimuth angles are equal to each other; the formula below is obtained with the cancellations as defined in [45].

$$H = \tan\lambda' . \tan\lambda \frac{L_{ps}}{\tan\lambda' - \tan\lambda} \qquad (5.5)$$

If the satellite elevation angle is 90 degrees, then the geometry becomes simple and only the triangle that is related with the sun angles is remained. Hence, the formula is obtained as:

$$H = \tan\lambda' . L_{sb} \qquad (5.6)$$

5.2 Experimental Results

The building height estimation from shadow algorithm is implemented by using MATLAB. Since the satellite angles are not available for the sample images, only the sun angles are used in the calculation process. Hence, sample images are selected from the image, which have satellite elevation angles close to 90 degrees.

Below the graphical user interface of the program is presented:

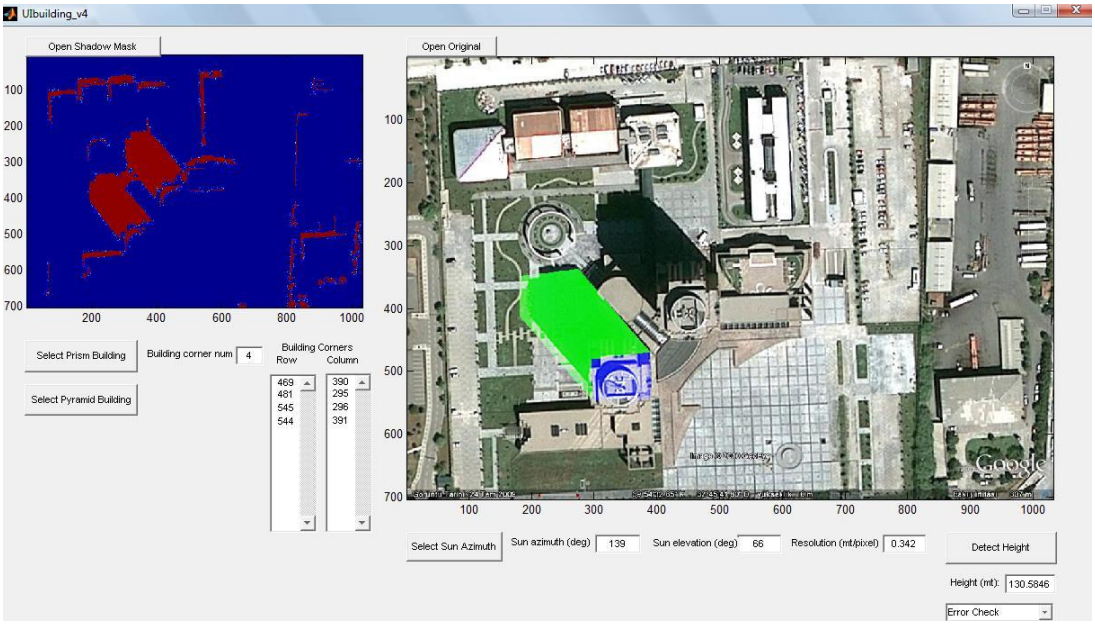

Figure 96 – User interface for building height estimation program

The input to the process is the original image and the detected shadow mask of this image. Building detection is beyond the scope of this thesis so one assumption is the buildings are already detected by a prior process. So the building corners are defined by the user.

After defining the building corners, the sun angles should be input by the user. If the sun angle are not available for an image, which was the case for the experimented sample images, a simple way to determine these angles are defined herein. For determining sun angles from a sample image, one should at least know the image date and time. There are astronomical formulas to determine the sun angle and there are internet sites that return the sun elevation and azimuth angles by using the location information, date and time. There are a number of sun angle providers and for this work the tables are got from National Research Council Canada web site [http://www.nrc-cnrc.gc.ca].

However, for the sample image case, the time information is also absent. Hence, the following procedure is applied to determine the angles: Assuming that the north direction is available, firstly, the angle between north and shadow edge is measured. By using this information, the sun azimuth the angle is found by subtracting 180 degrees from that angle. Then using this angle information, the time is obtained from the available sun angles table for the relevant location and date. Once the time has found, the sun elevation angle can also be obtained. For example for the sample image in Figure 96 above, the following table is valid for the given location and the dates.

Table 4 – Sun angles table for the sample image 1 location and date

Time	Hour Angle	Solar Altitude	Solar Azimuth	Shadow Length Factor
4:45	-7.17	0.5	63.2	112.97
5:00	-6.92	3.1	65.5	18.46
5:15	-6.67	5.7	67.9	9.94
5:30	-6.42	8.4	70.1	6.75
5:45	-6.17	11.2	72.4	5.07
6:00	-5.92	13.9	74.6	4.04
6:15	-5.67	16.7	76.8	3.33
6:30	-5.42	19.5	79.0	2.82
6:45	-5.17	22.3	81.2	2.43
7:00	-4.92	25.2	83.5	2.13
7:15	-4.67	28.1	85.8	1.88
7:30	-4.42	30.9	88.1	1.67
7:45	-4.17	33.8	90.5	1.49
8:00	-3.92	36.7	92.9	1.34
8:15	-3.67	39.6	95.5	1.21
8:30	-3.42	42.4	98.2	1.09
8:45	-3.17	45.2	101.1	0.99
9:00	-2.92	48.1	104.1	0.90
9:15	-2.67	50.8	107.5	0.81
9:30	-2.42	53.5	111.1	0.74
9:45	-2.17	56.2	115.1	0.67
10:00	-1.92	58.7	119.6	0.61
10:15	-1.67	61.2	124.6	0.55
10:30	-1.42	63.5	130.4	0.50
10:45	-1.17	65.5	136.9	0.45
11:00	-0.92	67.4	144.5	0.42

Table 4 – (continued)

Time	Hour Angle	Solar Altitude	Solar Azimuth	Shadow Length Factor
11:15	-0.67	68.9	153.0	0.39
11:30	-0.42	70.0	162.5	0.36
11:45	-0.17	70.6	172.7	0.35
12:00	0.08	70.7	183.3	0.35
12:15	0.33	70.2	193.8	0.36
12:30	0.58	69.3	203.6	0.38
12:45	0.83	68.0	212.5	0.40
13:00	1.08	66.3	220.4	0.44
13:15	1.33	64.3	227.3	0.48
13:30	1.58	62.1	233.3	0.53
13:45	1.83	59.7	238.6	0.59
14:00	2.08	57.2	243.3	0.65
14:15	2.33	54.5	247.5	0.71
14:30	2.58	51.8	251.2	0.79
14:45	2.83	49.1	254.7	0.87
15:00	3.08	46.3	257.8	0.96
15:15	3.33	43.5	260.8	1.05
15:30	3.58	40.6	263.5	1.17
15:45	3.83	37.8	266.1	1.29
16:00	4.08	34.9	268.6	1.43
16:15	4.33	32.0	271.0	1.60
16:30	4.58	29.1	273.4	1.79
16:45	4.83	26.3	275.7	2.03
17:00	5.08	23.4	277.9	2.31
17:15	5.33	20.6	280.1	2.67
17:30	5.58	17.7	282.4	3.12
17:45	5.83	14.9	284.6	3.75
18:00	6.08	12.2	286.8	4.63
18:15	6.33	9.4	289.0	6.01
18:30	6.58	6.7	291.3	8.46
18:45	6.83	4.1	293.6	14.01
19:00	7.08	1.5	295.9	38.98

Since the image is in north up orientation, sun azimuth angle is obtained from the shadow edge as 138 degrees. Then, from the table, one could determine that the sun elevation angle by linear interpolation between 10:45 and 11:00, to be approximately equal to 66 degrees.

After obtaining sun angles, the final step is calculation of the building height. The calculation process is automatically achieved and the algorithm iteratively constitutes the shadow from the building corners and shadow azimuth angle. Once the shadow mask and constituted shadow is fitted,

then the shadow length is returned. There are two methods in the proposed algorithm to fit to the shadow mask. One approach is checking the error between shadow mask and shadow and stopping when the error starts to increase. The other is checking only the coinciding pixels and stopping when the coinciding pixel number is no more increased.

The resulting shadow length in pixels is then converted to meters by using the image scale. From this detected shadow length, the building height is calculated by the formula in (5.6).

The reference building heights are collected from Emporis company's web site [www.emporis.com]. This company is a global provider for building related information.

The experimental results are given below for the sample satellite images:

Table 5 – Building height estimation results

SCENE	Ref. height (mt)	Calc. height (mt)	Error (mt)	Error (%)
akman	110	108,8	1,2	1,1%
atakule	125	140,8	15,8	12,6%
calisma	100	87,7	12,3	12,3%
dışişleri	67	73,5	6,5	9,7%
dikmen	140	142,3	2,3	1,6%
grand hotel	65	71,5	6,5	10,0%
halkbank	123,14	130,2	7,1	5,7%
hazine	90	91,8	1,8	2,0%
isbank	181,2	124,4	56,8	31,3%
mkek	55	54,0	1,0	1,8%
paris	300	306,0	6,0	2,0%
portakal	160	154,4	5,6	3,5%
sabanci	98,35	106,5	8,2	8,3%
sheraton	143	101,0	42,0	29,4%
tedaş	70	69,5	0,5	0,7%
tobb kule	140	130,6	9,4	6,7%

The experiment on real images could be done by not considering the satellite angles, since this information is not available. So in addition to real satellite image based experiments, a home setup is also established, where the sun and satellite are simulated by a ceiling lamb and a hand held camera with a tripod respectively. The building is simulated by a rectangular prism object. Three cases are experimented and the formulas given in (5.6) is used for the first case and (5.4) is used for the other cases, to calculate the objects height. The objects measured height is 28.4 cm. The setup is given below and results are given in Table 6:

Figure 97 – The simulation of different satellite azimuth and elevation angles (left: scene 1, middle: scene 2, right: scene 3)

Table 6 – The results of simulation of different satellite azimuth and angles

	Light source angles (deg)		Camera angles (deg)		Calculated Height using (5.4)	Error using (5.4)	Calculated Height using (5.6)	Error using (5.6)
	Azi.	Elev.	Azi.	Elev.				
Scene 1	20	55	0	90	28.56 cm	0.56%	Not applicable	-
Scene 2	20	55	39	48	19.62 cm	30.9%	28.77 cm	1.3%
Scene 3	20	55	180	69	51.27 cm	80,5%	26.03 cm	8.35%

5.3 Discussion about Building Height Estimation Results

Building height estimation from shadow using the method defined in previous section usually gives satisfactory results. The error percentage is usually less than 10%. However, for the cases that satellite elevation angle differs much from 90 degrees then the error starts to increase.

An important issue is the dependency of the method on shadow detection result; hence, a successful detection is also an important input to have as a prior step before building height estimation. Erroneous detections will eventually lead to unsatisfactory height estimations.

Also it should be noted that the overlapping shadows may degrade the performance since the building shadow length may not be calculated truly.

The tested method on real satellite images using (5.4) is applicable successfully to the images where the satellite elevation angles close to perpendicular to the earth normal.

In the experiment that simulates the satellite and sun angle, one could observe that using the formula (5.4) gives unacceptable results for camera elevation angles different than 90 degrees. However, if the correct formula for this case (5.6) is applied the results are much better.

As a concluding remark, for the satellite images that has satellite elevation angles perpendicular to the earth normal the simple formula given in (5.4) could be used. However if the satellite elevation differs from 90 degrees than the formula given in (5.6) should be used which considers all the sun and satellite angles.

CHAPTER 6

CONCLUSIONS

6.1. Summary of the thesis

In this thesis, shadow detection in aerial images and compensation of the detected shadow regions are addressed. In addition, an example application of shadow detection, building height estimation, is also mentioned.

Firstly, the shadow definition has been made and referred color spaces are explained. Shadows occur when the light is occluded by some other object. Shadow regions are the parts of an image that is illuminated only by ambient light, but not by direct sun light. If the shadow appears on the object itself it is called self shadow, otherwise it is called cast shadow [3], [28], [38]. There are different color spaces that each one has different property and used for different purposes. For example, the RGB color space is mainly used for display purposes. However, HSI or HSV color space is preferred in most of the shadow detection methods, since beneficial shadow features could be extracted from these color space.

Secondly, the shadow features are analyzed and the shadow detection methods are overviewed. Obviously the intensity will be less in shadow regions. So the component in a color space that represents the intensity will be small in shadow regions, like the value component in HSV color space or Y component in YIQ color space. The Hue and Saturation components of HSI/HSV color space are also mentioned to be increased in aerial and satellite images [4], [34], [36]. From the analyzed shadow features, novel shadow detection approaches are proposed. With these proposed approaches, some feature based shadow detection methods are analyzed

in detail. Then novel methods and selected shadow detection methods are compared with sample images. One sample image was an indoor image with a shadow mask ground truth. The results of the methods are compared quantitatively. In addition, two aerial images are used for a qualitative comparison.

Shadow compensation methods are also overviewed in this thesis. Histogram matching, gamma correction and linear correlation are experimented on some sample images. Histogram matching is the process where the histogram of an input image is aimed to match a specified histogram. Cumulative histogram of input image and specified histogram is used for the matching. The grey values of input image are mapped to the output grey values where their cumulative histogram values are the same [54]. The histogram matching could be done globally, for the whole image, or it could be done locally, between a connected shadow region and its non-shadowed neighbor region. If only the intensity would be compensated, the HSV color space value component's histogram is matched. However, if color distortion should also be aimed to compensated, then all the components' histograms are matched separately. Gamma correction process, which is mainly used to compensate the nonlinear response of display devices like CRT, has also proposed for shadow compensation [9]. The gamma value is selected by trial and error method. Beside these methods, linear correlation is also another proposed method [9] for shadow compensation. These methods are tested on sample images and the results are compared.

Finally, a shadow detection application example is studied. Building height estimation is one of the applications that uses detected shadow information. In this application, firstly shadow length is measured. Then by using azimuth and elevation angles of sun and satellite, the building height is estimated. The method has a simplified formula for the case that satellite elevation angle is perpendicular. For the sample images that are tested, the satellite angles were not available. So the images are selected to be the ones that have nearly 90 degrees of satellite elevation. However, a home setup is also

experimented for the case where satellite elevation differs from perpendicular.

6.2. Discussion

In the shadow features part, the different color spaces are experimented on six different uniformed color sample images. The tested colors are yellow, black, blue, green, red and white. In the RGB color space case, all the color space components are decreased as expected, since the illumination is decreased. However, a method to separate the shadow and non-shadow regions could not be found in the literature, and also could not able to be proposed. One important observation on white colored sample image is the one that, blue is the less attenuated than green and red is most attenuated component. This issue is also mentioned in the literature as Rayleigh scattering effect [11]. In the HSV color space, it is observed that value component decreases and saturation increases for all the cases. However the hue component stays constant for yellow, green and blue cases, and increases in black, red and white cases. By considering these properties, several methods are proposed in the literature [4], [34], [35], [36]. Beside these methods, novel approaches are proposed in this thesis. Another color space is YIQ, which is observed. In this case, the Y component is decreased since it represents the illumination and the other two components that represent the color information stays constant. Finally, $C_1C_2C_3$ color space is observed in these sample images, but no beneficial deduction could be extracted. From these observations, it is deducted that HSV color space is a suitable choice for shadow detection.

In the shadow detection part of the thesis, some threshold based methods in the literature [4], [34], [35], [36] and novel proposed methods are observed on the same six uniform color image samples. It is observed that for none of the methods, except $(H+S+1)/(V^2+V+1)$ ratio threshold based approach, it is possible to set a single threshold. Also the separation value is defined, which shows performance of the methods separation of shadow and non-shadow regions. It is observed that the (I-S) difference [35] and the $(H+S+1)/(V^2+V+1)$ ratio threshold based approaches performed better

separation values. After these experiments on uniform colored sample images, some feature based methods [3], [4], [34], [35], [36] from the literature and some novel approaches are experimented on a indoor scene and two aerial images. From these experiments, it is observed that, one of the novel proposed method, $(H+S+1)/(V^2+V+1)$ ratio threshold, not only has superior results for the quantitative comparison case, but also output satisfactory shadow detection results in both aerial image samples. Eventually, from these experiments and observations, it could be deducted that $(H+S+1)/(V^2+V+1)$ ratio threshold could be a choice for shadow detection on aerial images.

In the shadow compensation part, histogram matching, gamma correction and linear correlation are experimented on some sample images. It is observed that local histogram matching on all components of HSV color space performed superior results. However, none of the methods could able to compensate the shadow region satisfactorily for all the cases.

Finally, building height estimation as an example of the application to shadow detection, is studied. An equation has been extracted from the triangles constituted by the building, sun and satellite angles [56]. This equation has simplified versions for sun and satellite azimuth angles are the same [45] and satellite angle is 90 degrees. In this part, it is observed that the simplest form of the equation could be used for the cases that satellite angle is approximately 90 degrees, with an error less than 10%. However, the error increases when satellite angle differs from 90 degrees. In this case, if the original equation [44] is used then the error again decreases to acceptable values. The shadow length in these experiments, are calculated with a method based on [57]. Eventually, it could be deducted that for a given aerial image, it is possible to estimate a buildings height from its shadow length, by using the azimuth and elevation angles of sun and satellite.

6.3. Future Work

As future work, edge based shadow detection methods could also be studied, beside the threshold based approaches. In addition, threshold based approaches could be studied, whether that methods also be used for shadow edge detection. Adaptive thresholds could also be studied in shadow detection algorithms.

In shadow compensation part of this study, local histogram matching, gamma correction and linear correlation based approaches are applied on a shadow region and its shadow buffer zones constituted from neighbor pixels. As a future study, instead of selecting neighbor pixels, image regions which are the same class of surface type with shadowed part, could be selected as input to shadow compensation. Also other shadow compensation methods in the literature could be experimented and compared with these methods.

Finally, using satellite images with all the sun and satellite angles are given; building height estimation could be revisited using the equation (5.4) that considers all the angles.

REFERENCES

[1] Y. Li, T. Sasagawa, P. Gong, “A System of the Shadow Detection and Shadow Removal for High Resolution City Aerial Photo”, ISPRS Congress Istanbul, Vol. 35, Comm. III, 2004

[2] B. B. Madhavan, T. Kikuo, T. Sasagawa, H. Okada, Y. Shimozuma, “Automatic Extraction Of Shadow Regions In High-Resolution ADS40 Images - By Robust Approach of Feature Spaces Analysis” ISPRS Congress Istanbul, Vol. 35, Comm. III, 2004

[3] H. Etemadnia, M. R. Alsharif, “Automatic Image Shadow Identification using LPF in Homomorphic Processing System” VIIth Digital Image Computing: Techniques and Applications (DICTA), 2003

[4] H. Ma, Q. Qin, X. Shen, “Shadow Segmentation And Compensation In High Resolution Satellite Images” IEEE International Geoscience & Remote Sensing Symposium (IGARSS), 2008

[5] M. Xiao, C. Z. Han, L. Zhang, “Moving Shadow Detection and Removal for Traffic Sequences” International Journal of Automation and Computing, January 2007, p. 38-46, 2007

[6] L. Landabaso, M. Pardàs, L. Q. Xu, “Shadow Removal with Morphological Reconstruction”, ICASSP, p. 729-732, 2005

[7] G. D. Finlayson, S. D.Hordley, M. S. Drew, “Removing Shadows Using Retinex”, IS&T/SID Tenth Color Imaging Conference, 2002

[8] E. Salvador, A. Cavallaro, T. Ebrahimi “Shadow Identification And Classification Using Invariant Color Models”, ICASSP, 2001

[9] P. Sarabandi, F. Yamazaki, M. Matsuoka, A. Kiremidjian, “Shadow Detection And Radiometric Restoration In Satellite High Resolution Images”, IGARSS, 2004

[10] G. D. Finlayson, S. D. Hordley, M. S. Drew, “Removing Shadows from Images”, 7th European Conference on Computer Vision-Part IV, 2002

[11] S. M. Adler-Golden, M. W. Matthew, G. P. Anderson, G. W. Felde, J. A. Gardner, “An Algorithm For De-Shadowing Spectral Imagery”, Earth Sciences and Applications Workshop, 2002

[12] A. Prati, I. Mikic, M. M. Trivedi, R. Cucchiara, “Detecting Moving Shadows: Algorithms and Evaluation”, IEEE Transactions on Pattern Analysis and Machine Intelligence, Vol. 25, No. 7, 2003

[13] J. M. Scanlan, D. M. Chabries, R. W. Christiansen, “A Shadow Detection and Removal Algorithm for 2D Images”, International Conference on Acoustics, Speech, and Signal Processing (ICASSP), 1990

[14] M. D. Levine, J. Bhattacharyya, “Removing Shadows”, Pattern Recognition Letters, Vol. 26 , Issue 3, p. 251-265, 2005

[15] J. Yao, Z. Zhang, “Systematic Static Shadow Detection”, 17th International Conference on Pattern Recognition (ICPR), 2004

[16] K. Barnard, G. Finlayson “Shadow Identification using Colour Ratios”, IS&T/SID Eighth Color Imaging Conference: Color Science, Systems and Applications, p. 97-101, 2000

[17] R. Jain, R. Kasturi, B.G. Schunck, “Machine Vision”, McGraw Hill, 1995

[18] Y. Matsushita, K. Nishino, K. Ikeuchi, M. Sakauchi, “Illumination Normalization with Time-Dependent Intrinsic Images for Video Surveillance”, IEEE Transactions on Pattern Analysis and Machine Intelligence (TPAMI), Vol. 26, Issue:10, p.1336-1347, 2004

[19] A. Leone, C. Distante, F. Buccolieri, “A Texture-Based Approach For Shadow Detection”, Advanced Video and Signal Based Surveillance, (AVSS), 2005

[20] D. J. Kriegman, P. N. Belhumeur, “What shadows reveal about object structure”, European Conference on Computer Vision, Vol. II, p. 399-414, 1998

[21] M. A. Güler, “Detection Of Earthquake Damaged Buildings From Post Event Photographs Using Perceptual Grouping”, Ms. Thesis, METU, 2004

[22] L. Havasi, T. Szirányi, M. Rudzsky, “Adding Geometrical Terms To Shadow Detection Process”, 14th European Signal Processing Conference (EUSIPCO), 2006

[23] A. J. Joshi, S. Atev, O. Masoud, N. Papanikolopoulos, “Moving Shadow Detection with Low- and Mid-Level Reasoning”, IEEE International Conference on Robotics and Automation, 2007

[24] S. Müller, D. W. Zaum, “Robust Building Detection In Aerial Images”, ISPRS Workshop CMRT ’05, p. 143–148, 2005

[25] A. Leone, C. Distante, F. Buccolieri, “Shadow Detection for Moving Objects Based on Texture Analysis”, Pattern Recognition, Vol. 40 , Issue 4, p. 1222-1233, 2006

[26] J. J. Yoon, C.Koch, T. J. Ellis, “Shadow Flash: An Approach for Shadow Removal in an Active Illumination Environment”, 13th British Machine Vision Conference University of Cardiff , 2002

[27] Y. Weiss, “Deriving Intrinsic Images from Image Sequences”, IEEE International Conference on Computer Vision (ICCV), 2001

[28] P. M. Dare, “Shadow Analysis in High-Resolution Satellite Imagery of Urban Areas”, Photogrammetric Engineering and Remote Sensing, Vol. 71, pp. 169-177, 2005

[29] C. Fredembach, G. Finlayson, “Simple Shadow Removal”, International Conference of Pattern Recognition (ICPR), 2006

[30] G. Finlayson, M. Drew, C. Lu, “Intrinsic Images by Entropy Minimization”, 8th European Conference on Computer Vision (ECCV), 2004

[31] C. Fredembach, G. Finlayson, “Hamiltonian Path Based Shadow Removal”, IEEE Transactions on Image Processing, Vol. 17, Issue: 4, p. 608-621, 2008

[32] A. Suzuki, A. Shio, H. Ami, S. Ohtsuka, “Dynamic Shadow Compensation of Aerial Images Based on Color and Spatial Analysis”, 15th International Conference on Pattern Recognition (ICPR), 2000

[33] X. Gu, D. Yu, L. Zhang, “Image Shadow Removal Using Pulse Coupled Neural Network”, IEEE Transactions on Neural Networks, Vol. 16, No. 3, 2005

[34] V. J. D. Tsai, “A Comparative Study on Shadow Compensation of Color Aerial Images in Invariant Color Models”, IEEE International Geoscience & Remote Sensing Symposium (IGARSS), 2006

[35] A. M. Polidorio, F. C. Flores, N. N. Imai, A. M. G. Tommaselli, C. Franco, “Automatic Shadow Segmentation in Aerial Color Images” XVI Brazilian Symposium on Computer Graphics and Image Processing (SIBGRAPI), 2003

[36] J. Huang, W. Xie, L. Tang, “Detection of and compensation for shadows in colored urban aerial images”, 5th World Congress on Intelligent Control and Automation, 2004

[37] B.T. Phong, “Illumination for Computer Generated Pictures”, Communications of the ACM, 1975

[38] C. Jiang, M. O. Ward, “Shadow Identification”, IEEE Conference on Computer Vision and Pattern Recognition (ICCVPR), 1992

[39] T. P. Wu, C. K. Tang, “A Bayesian Approach for Shadow Extraction from a Single Image”, IEEE International Conference on Computer Vision (ICCV), 2005

[40] M. A. Berbar, S. F. Gaber, “Clouds And Shadows Detection And Removing From Remote Sensing Images”, International Conference on Electrical, Electronic and Computer Engineering (ICEEC), 2004

[41] James J. Simpson, James R. Stitt, “A Procedure for the Detection and Removal of Cloud Shadow from AVHRR Data over Land”, IEEE Transactions On Geoscience And Remote Sensing, 1998

[42] T. Gevers, A. W. M. Smeulders, “Color Based Object Recognition” Image Analysis and Processing Lecture Notes in Computer Science, Vol. 1310, p. 319-326, 1997

[43] T. Acharya, A. K. Ray, “Image Processing Principles and Applications”, 2005

[44] A. Massalabi, D. C. He, G. B. Bénié, E. Beaudry, “Detecting Information Under and from Shadow in Panchromatic Ikonos Images of The City of Sherbrooke”, IEEE International Geoscience & Remote Sensing Symposium (IGARSS), 2004

[45] W. Ding, F. Zhu, Y. Hao, “Interactive 3D City Modeling using Google Earth and Ground Images” Fourth International Conference on Image and Graphics (ICIG), 2007

[46] R. Bolter, “Reconstruction of Man-Made Objects from High Resolution SAR Images”, IEEE Aerospace Conference, 2000

[47] E. Salvador, A. Cavallaro, T. Ebrahimi, “Cast Shadow Segmentation Using Invariant Color Features”, Computer Vision and Image Understanding, Vol. 95, Issue 2, p. 238-259, 2004

[48] V. J. D. Tsai, “Automatic Shadow Detection and Radiometric Restoration on Digital Aerial Images”, IEEE International Geoscience & Remote Sensing Symposium (IGARSS), 2003

[49] Z. Cai, A. T. S. Ho, “Cloud Detection and Removal in Satellite Images for Tropical Regions”, Proceedings of ICSP, 1996

[50] A. Prati, I. Miki, R. Cucchiara, M. M. Trivedi, “Comparative Evaluation of Moving Shadow Detection Algorithms”, IEEE CVPR workshop on Empirical Evaluation Methods in Computer Vision, 2001

[51] C. Lu, M. S. Drew, “Shadow Segmentation and Shadow-Free Chromaticity via Markov Random Fields”, CIC13: Color Imaging Conference, Scottsdale, 2005

[52] G. Junxiang, T. Yan, L. Yong, “Ellipsoidal Method for Shadow Detection Based on Normalized RGB Values”, International Conference on Networking and Digital Society, 2009

[53] J. Tian, J. Sun, Y. Tang, “Tricolor Attenuation Model for Shadow Detection”, IEEE Transactions on Image Processing, Vol. 18, Issue 10, 2009

[54] R. C. Gonzalez, R. E. Woods, “Digital Image Processing, 2nd edition”, 2002

[55] N. Otsu, “A Threshold Selection Method from Gray Level Histograms”, IEEE Transactions on Systems, Man, and Cybernetics, Vol. Smc-9, No. 1, 1979

[56] C. Lin, R. Nevatia, “3-D Descriptions of Buildings from an Oblique View Aerial Image”, International Symposium on Computer Vision, 1995

[57] T. Kim, T. Javzandulam, T. Y. Lee, “Semiautomatic Reconstruction of Building Height and Footprints from Single Satellite Images”, IEEE International Geoscience & Remote Sensing Symposium (IGARSS), 2007